THE ASTROPHYSICAL JOURNAL, 550:212–229, 2001 March 20

STELLAR MASS-TO-LIGHT RATIOS AND THE TULLY-FISHER RELATION

ERIC F. BELL AND ROELOF S. DE JONG[1]
Steward Observatory, University of Arizona, 933 N. Cherry Avenue, Tucson, AZ 85721; ebell@as.arizona.edu, rdejong@as.arizona.edu
Received 2000 August 18; accepted 2000 November 21

ABSTRACT

We have used a suite of simplified spectrophotometric spiral galaxy evolution models to argue that there are substantial variations in stellar mass-to-light (M/L) ratios within and among galaxies, amounting to factors of between 3 and 7 in the optical and factors of 2 in the near-infrared. Our models show a strong correlation between stellar M/L and the optical colors of the integrated stellar populations. Under the assumption of a universal spiral galaxy initial mass function (IMF), relative trends in model stellar M/L with color are robust to uncertainties in stellar population and galaxy evolution modeling, including the effects of modest bursts of star formation. Errors in the dust-reddening estimates do not strongly affect the final derived stellar masses of a stellar population. We examine the observed maximum disk stellar M/L ratios of a sample of spiral galaxies with accurate rotation curves and optical and near-infrared luminosity profiles. From these observed maximum disk M/L ratios we conclude that a Salpeter IMF has too many low-mass stars per unit luminosity but that an IMF similar to the Salpeter IMF at the high-mass end with less low-mass stars (giving stellar M/L ratios 30% lower than the Salpeter value) is consistent with the maximum disk constraints. Trends in observed maximum disk stellar M/L ratios with color provide a good match to the predicted model relation, suggesting that the spiral galaxy stellar IMF is universal and that a fraction of (particularly high surface brightness) spiral galaxies may be close to maximum disk. We apply the model trends in stellar M/L ratio with color to the Tully-Fisher (T-F) relation. We find that the stellar mass T-F relation is relatively steep, has modest scatter, and is independent of the passband and color used to derive the stellar masses, again lending support for a universal IMF. The difference in slope between the optical (especially blue) and near-infrared T-F relations is due to the combined effects of dust attenuation and stellar M/L variations with galaxy mass. Assuming the *Hubble Space Telescope* Key Project distance to the Ursa Major Cluster and neglecting the (uncertain) molecular gas fraction, we find that the baryonic T-F relation takes the form $M_{\rm baryon} \propto V^{3.5}$ (with random and systematic 1 σ slope errors of ~ 0.2 each) when using a bisector fit and rotation velocities derived from the flat part of the rotation curve. Since we have normalized the stellar M/L ratios to be as high as can possibly be allowed by maximum disk constraints, the slope of the baryonic T-F relation will be somewhat shallower than 3.5 if all disks are substantially submaximal.

Subject headings: dust, extinction — galaxies: evolution — galaxies: kinematics and dynamics — galaxies: spiral — galaxies: stellar content

On-line material: machine-readable tables

1. INTRODUCTION

The stellar mass-to-light (M/L) ratio is an important parameter in astrophysics as it allows translation between photometry and dynamics. The stellar M/L ratio has a direct bearing on two hotly debated areas in spiral galaxy research: the appropriate stellar M/L ratios to be used for spiral galaxy rotation curve decompositions and the passband-dependent slope of the galaxy magnitude–rotation velocity relation (or Tully-Fisher [T-F] relation; Tully & Fisher 1977). In this paper we address the stellar M/L ratios of spiral galaxies, briefly explore the implications of our results for rotation curve decompositions, and investigate in more depth the slope of the T-F relation.

There is currently much interest in decomposing spiral galaxy rotation curves into contributions from the gaseous, stellar, and dark matter contents (e.g., Verheijen 1997; de Blok & McGaugh 1998). The primary motivation for this interest is that, in principle, the structure of dark matter halos can be determined from spiral galaxy rotation curves *if* the contribution from gas and stars can be properly understood. In turn, the structure of dark matter halos is a strong constraint on dark matter halo formation models (e.g., Moore et al. 1998; Navarro & Steinmetz 2000a). The main challenge in determining the dark matter contribution to a given rotation curve is our ignorance regarding plausible values of the stellar M/L ratio: the gas contribution is typically well understood and relatively small (Verheijen 1997; Swaters, Madore, & Trewhella 2000). The situation is degenerate enough that many rotation curves can be equally well fitted by models in which the central parts of the rotation curve are dominated entirely by stellar mass or by dark matter (e.g., van Albada et al. 1985; Swaters 1999). In order to resolve this degeneracy, some independent constraints on stellar M/L ratios, as well as their variations with radius and galaxy properties, are required.

The implications of the stellar M/L ratio for the T-F relation are no less important. The T-F relation relates the integrated luminosity in a given passband to the global dynamics of the galaxy and its dark matter halo. The dust-corrected T-F relation has a slope that steepens toward redder passbands (going between $L \propto V^3$ or shallower in the optical and $L \propto V^4$ in the near-infrared; Verheijen 1997; Tully et al. 1998), indicating that there is a trend in

[1] Hubble Fellow.

color and stellar M/L ratio with galaxy mass. This change in slope with passband can considerably weaken the power of the T-F relation as a test of galaxy formation and evolution models (such as those by Cole et al. 2000; Navarro & Steinmetz 2000b; van den Bosch 2000): it is possible to reproduce the T-F relation in one passband easily without reproducing the T-F relation in other passbands (for a multi–wave band comparison of models with the T-F relation see, e.g., Heavens & Jimenez 1999).

One way around this confusion is to explore the total baryonic mass T-F relation. An estimate of the baryonic T-F relation can be obtained by adding the gas mass to a crude estimate of stellar mass implied by the luminosity (usually assuming a constant M/L ratio). This has been attempted the most thoroughly by McGaugh et al. (2000) using a constant M/L ratio in B, I, H, and K bands, although, e.g., Milgrom & Braun (1988) and Matthews, van Driel, & Gallagher (1998) discussed aspects of this problem. Because the stellar M/L ratio is likely to vary along the T-F relation in all passbands, their composite baryonic T-F relation will have a larger scatter and different slope than the true baryonic T-F relation. A deeper and firmer understanding of the baryonic T-F relation is only possible once variations in stellar M/L ratio along the T-F relation are understood and incorporated in the analysis.

In this paper we use simplified spiral galaxy evolution models similar to the ones presented by Bell & Bower (2000) to investigate plausible trends in stellar M/L ratio with galaxy properties, assuming a universal initial mass function (IMF). We discuss these models briefly in § 2. In § 3 we investigate trends in spiral galaxy stellar M/L ratio for a number of plausible models, finding that there are systematic variations in stellar M/L ratio as a function of many galaxy parameters and that stellar M/L ratios correlate most tightly with galaxy color. In § 4 we investigate the physical basis of the color-M/L relation and we discuss uncertainties in the stellar M/L ratios, including the effects of using different stellar population models, different IMFs, different galaxy evolution prescriptions, and dust. In § 5 we discuss the implications of these variations in stellar M/L ratio for rotation curve decompositions and put the stellar M/L ratios onto an observationally determined maximum disk scale. In § 6 we then discuss at length the implications of these variations in stellar M/L ratio for the stellar mass and baryonic T-F relation. Finally, in § 7 we present our conclusions. Readers not interested in the details of the models and a detailed analysis of the uncertainties in model stellar M/L ratios can skip §§ 2 and 4. Note that we state all stellar M/L ratios in solar units. We adopt the *Hubble Space Telescope* (*HST*) Key Project distance scale in this paper, corresponding to $H_0 = 71$ km s^{-1} Mpc^{-1} (Sakai et al. 2000).

2. THE GALAXY EVOLUTION MODELS

To construct the model M/L ratios for spiral galaxies, we use models similar to those presented by Bell & Bower (2000). They presented a suite of simple spectrophotometric disk evolution models designed to reproduce many of the trends between the radially resolved colors of spiral galaxies and their structural parameters, as observed by Bell & de Jong (2000). These models were not designed to address the evolution of bulges or dwarf spheroidal galaxies: the star formation laws used in these models (parameterized using surface density) are valid only for disk-dominated galaxies. These models describe the evolution of a gaseous disk, according to a prescribed star formation law and chemical evolution prescription (assuming the instantaneous recycling approximation [IRA]). Relaxing the IRA would have two effects: it would allow nonsolar abundance ratios to develop, and it would slightly modify the time evolution of the metallicity of galaxies. Most stellar population models are incapable of dealing adequately with nonsolar abundance ratios; however, it looks likely that the effects of nonsolar abundance ratios on integrated colors are modest (as they mimic the effects of modest changes in metallicity; e.g., Salasnich et al. 2000). Furthermore, the time evolution of spiral galaxy metallicity (which is dominated, by mass, by the Type II supernova product oxygen) is described fairly accurately by the IRA except at late stages of galactic evolution near gas exhaustion (e.g., Tinsley 1980; Pagel 1998; Portinari & Chiosi 1999; Prantzos & Boissier 2000). Thus, our use of the IRA is a reasonable approximation, bearing in mind the modest effects caused by adopting it and the considerable stellar population and galaxy evolution modeling uncertainties.

To construct radially resolved stellar population colors, the stellar population synthesis (SPS) models of A. G. Bruzual & S. Charlot (2001, in preparation), as described in Liu, Charlot, & Graham (2000), are used, adopting a Salpeter (1955) IMF, which we modify by globally scaling down its stellar M/L ratio by a factor of 0.7 (see Fukugita, Hogan, & Peebles 1998). We adopt lower and upper mass limits of 0.1 and 125 $M_\odot$, respectively. In Bell & Bower (2000) we adopted a pure Salpeter (1955) IMF; in this paper we have been forced to adopt an IMF with lower M/L ratios to agree with observational maximum disk M/L constraints (see § 5). This global reduction in stellar M/L ratio is essentially the same as adopting an IMF with fewer low-mass stars, as the low-mass stars contribute only to the mass, but not to the luminosity or color, of the stellar population. It is interesting to note that there is increasing empirical evidence for a universal IMF with a Salpeter slope for stars more massive than the Sun and a shallower slope for stars less massive than the Sun (Kroupa 2000). This IMF has stellar M/L ratios comparable to or slightly lower than the maximum disk–scaled IMF that we adopt in this paper. It is important to note that neither the slope, nor the scatter of the stellar M/L ratios, nor the trends in color with galaxy properties are affected by our adoption of a scaled-down Salpeter IMF: the only effect on the following analysis is to modify the overall normalization of the stellar M/L ratios.

For our models, we follow the evolution of an exponential gaseous disk using either a Schmidt (1959) local gas density–dependent star formation law or a gas density– and dynamical time-dependent star formation law (Kennicutt 1998). Model galaxies with a wide range of masses and central surface densities are generated, as we do not attempt to predict a priori the mass and central surface density distributions of spiral galaxies. To avoid comparing the observed galaxies to model galaxies without any observed analog from Bell & de Jong (2000), we select model galaxies to have a similar range in K-band absolute magnitudes and central surface brightnesses as their observed galaxies (including an observed modest absolute magnitude–central surface brightness correlation). These models are tuned to reproduce observed trends in color-based local age and metallicity as a function of local K-band surface brightness, in conjunction with the observed correlation between gas

fraction and K-band central surface brightness (Bell & de Jong 2000; Bell & Bower 2000).

We present a total of six models in this paper. (1) We first use a closed-box model, with no gas infall or outflow, a galaxy age of 12 Gyr, and a Schmidt star formation law. The main disadvantages of this model are the lack of a strong metallicity-magnitude correlation and weaker age-magnitude correlation and the underprediction of the age gradients. We then allow (2) gas infall (whose timescale depends on galaxy mass and radius) *or* (3) metal-enriched outflow, both of which alleviate the above shortcomings of the closed-box model. (4) We then adopt a dynamical time-dependent star formation law (without infall or outflow), which we find produces a "backward" metallicity-magnitude correlation and is therefore unacceptable, in isolation. (5) We then explore the use of a mass-dependent galaxy formation epoch without infall or outflow, which imprints metallicity-magnitude and age-magnitude correlations. A mass-dependent formation epoch is a common feature of many cosmologically motivated galaxy formation models (e.g., Somerville & Primack 1999; Cole et al. 2000). (6) Finally, we explore a "burst" model with a mass-dependent galaxy formation epoch and no infall or outflow, where the star formation rate is varied on 0.5 Gyr timescales with a lognormal distribution with a factor of 2 width. None of these models perfectly describe the trends in spiral galaxy colors with galaxy parameters observed in Bell & de Jong (2000); however, the models taken as a suite encompass the range of behaviors seen in the observed galaxy sample. We adopt the mass-dependent formation epoch model with bursts, with a scaled-down Salpeter IMF, as the default model. This model reproduces the trends in local spiral galaxy age and metallicity with local K-band surface brightness with acceptable scatter, while simultaneously reproducing the age-magnitude and metallicity-magnitude correlations with acceptable scatter. However, as we later demonstrate (see, e.g., § 4.3 and Fig. 10), the choice of model does not significantly affect any of our conclusions. For more model details see Bell & Bower (2000).

3. CONSTRUCTING MODEL MASS-TO-LIGHT RATIOS

We use the spiral galaxy evolution models (which reproduce the trends in spiral galaxy color with structural parameters) to construct stellar M/L ratios for integrated stellar populations. These are converted into solar units assuming solar absolute magnitudes of 5.47, 4.82, 4.46, 4.14, and 3.33 in Johnson B and V, Kron-Cousins R and I, and Johnson K passbands, respectively (Cox 2000; Bessel 1979). We also adopt Johnson J- and H-band solar absolute magnitudes of 3.70 and 3.37, respectively, from Worthey (1994) as Cox (2000) does not present J- and H-band magnitudes of the Sun: Worthey (1994) magnitudes in other passbands are comparable to those presented by Cox (2000). Instead of using the full gas mass-loss histories from the SPS models, we used the IRA to construct the stellar masses. This may lead to errors of $\lesssim 5\%$ in stellar M/L ratio (compared to the exact value). Bearing in mind the size of variations in M/L ratio that the model predicts (greater than a factor of 2) and the other considerable uncertainties affecting the stellar M/L ratios, such as the stellar IMF and dust, our use of the IRA is more than acceptable.

We show an example of the stellar M/L ratios of our model galaxies for the mass-dependent formation epoch with bursts model in Figure 1. We show this particular model for two reasons. First of all, this model provides the best match to the overall observed galaxy properties. Secondly, and more importantly, this model shows the most scatter of any of our models but has quantitatively the same overall behavior as all of our models (see, e.g., § 4.3 and Fig. 10). We show the trends in stellar M/L ratio in the B band (*open circles*) and K band (*filled circles*) as a function of (*a*) K-band absolute magnitude, (*b*) K-band central surface brightness, (*c*) gas fraction, and (*d*) $B-R$ galaxy color. Results for other models are presented in the Appendix.

One obvious conclusion is that there are significant trends in model stellar M/L ratio with all four depicted galaxy parameters *in all passbands, even in the K band.* The trends amount to factors of ~ 7 in B, ~ 3 in I, and ~ 2 in K for plausible ranges of galaxy parameters. This firmly dispels the notion of a constant stellar M/L ratio for a spiral galaxy in any passband: this conclusion is even true in K band, where there have been claims that the stellar M/L ratio will be robust to differences in star formation history (SFH; e.g., de Jong 1996; Verheijen 1997). Of course, we find that the trends in stellar M/L ratio are minimized in K band: this suggests that K-band observations are important for any observations in which minimizing scatter in M/L ratio is important (e.g., for rotation curve studies).

The scatter in model stellar M/L ratio at a given magnitude is rather large as a consequence of the modeling assumptions. The SFH of our model galaxies depends primarily on their local surface density, and only weakly on their total mass, as is observed (Bell & de Jong 2000). As

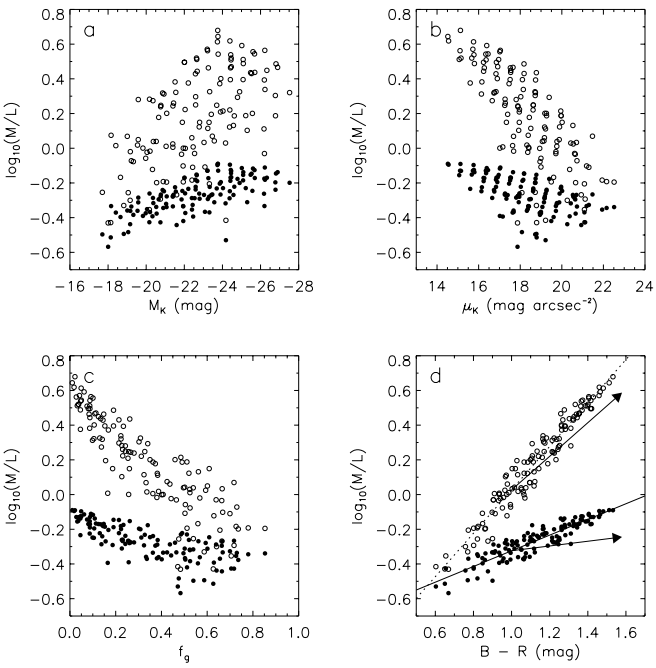

FIG. 1.—Trends in model stellar M/L ratios with galaxy parameters for the formation epoch model with bursts. We show the trends in model stellar M/L ratio in the B band (*open circles*) and K band (*filled circles*) as a function of (*a*) K-band absolute magnitude, (*b*) K-band central surface brightness, (*c*) gas fraction, and (*d*) $B-R$ galaxy color. In panel (*d*), we also show the fit to the variation of model stellar M/L ratio with $B-R$ color for this model in B (*dotted line*) and K band (*solid line*) and dust extinction vectors in B and K band (*arrows*) following Tully et al. (1998). The dust extinction vectors represent the correction to face-on suffered by a Milky Way–type galaxy viewed at an inclination of 80°.

galaxies come in a range of surface brightnesses at a given magnitude (de Jong & Lacey 2000), our models will have a range of SFHs and consequently M/L ratios at a given magnitude. There is considerable scatter in stellar M/L ratio with K-band central surface brightness and with gas fraction; however, this scatter is highly model dependent as there is no scatter in these relations for the closed-box models and intermediate scatter for the outflow and infall models.

One important conclusion is that, for all the models investigated for this paper, the model stellar M/L ratios in all optical and near-infrared (near-IR) passbands correlate strongly, with minimal scatter, with galaxy color (see also Bottema 1997). This is expected: the star formation and chemical enrichment history determine both the stellar M/L ratio and galaxy color. Later, we demonstrate that the slope of the M/L-color correlation is very robust, and we place a strong constraint on the zero point of the correlation. This correlation is a powerful tool for understanding stellar M/L ratios of spiral galaxies for use in, e.g., rotation curve decompositions or in constructing passband-independent T-F relations. We tabulate least-squares fits to the maximum disk–scaled color–stellar M/L ratio relations in Table 3 of the Appendix for all models introduced in § 2 and for a broad range in color combinations.

Using our models, we predict, *under the assumption of a universal IMF*, that workers determining the stellar M/L ratios of spiral galaxies (e.g., Bottema 1993, 1999; Swaters 1999; Weiner et al. 2001) will, with sufficient sample size and control of the systematic uncertainties, observe trends in stellar M/L ratio that correlate most tightly with galaxy color. In § 5 we demonstrate that there are already indications from rotation curve studies that the correlation between M/L ratio and color has been observed (see also Ratnam & Salucci 2000).

Another interesting implication of the tight correlation between stellar M/L ratio and color is that, because color gradients are common in spiral galaxies, significant gradients in stellar M/L ratio should be present in most spirals, in the sense that the outer regions of galaxies will tend to have lower stellar M/L ratios than the inner regions of galaxies (assuming a universal IMF). Obviously this stellar M/L ratio gradient will vary on a case-by-case basis. For many galaxies the assumption of a constant stellar M/L ratio over the disk will not significantly affect mass decompositions using rotation curves, as in the outer regions (where the stellar M/L ratio is lower) the stars contribute much less to the total mass than the dark matter (e.g., Weiner et al. 2001). Nevertheless, for accurate rotation curve studies, or studies based on, e.g., B-band photometry where the stellar M/L ratio varies strongly as a function of color, the radial variation of stellar M/L ratio should not be ignored. A detailed study of spiral galaxy rotation curves, using these model stellar M/L ratios, will be presented in our next paper.

4. HOW ROBUST ARE THE STELLAR MASS-TO-LIGHT RATIOS?

In the previous section we made some strong claims about the stellar M/L ratios of spiral galaxies. However, there are a number of uncertainties that may affect the model stellar M/L ratios, such as uncertainties in SPS and galaxy evolution models, dust, and most importantly, the stellar IMF (and possible trends in IMF with galaxy type and structure). In the next sections we discuss some of these uncertainties and the bearing of these on our results.

4.1. *The Origin of the Color-M/L Correlation*

Before we can assess the uncertainties in the model color-M/L relations, we have to understand why the correlation between color and stellar M/L ratio exists in the first place. To this end, we show in Figure 2 color versus stellar M/L ratio for a grid of exponentially declining star formation rate models. To construct model colors, we use SPS models with different metallicities from A. G. Bruzual & S. Charlot (2001, in preparation). We use exponentially declining star formation rates as models with this type of SFH can reproduce the optical–near-IR colors of spiral galaxies quite naturally (e.g., Bell & de Jong 2000). Furthermore, a slowly declining or constant SFH is inferred for the solar neighborhood (e.g., Rocha-Pinto et al. 2000). The exponential decline in star formation rate is parametrized by e-folding timescale τ, and the colors and M/L ratios are evaluated after a lifetime of 12 Gyr. Models with different τ but the same metallicity are connected by solid lines, while models with the same τ but different metallicities are connected by dashed lines.

When we consider the model grid for M/L ratio in the B band versus $B-R$ color (Fig. 2*a*), we can immediately see why the B-band stellar M/L ratio–color relation works so well. There is a tight correlation between $B-R$ color and stellar M/L ratio independent of metallicity or SFH. Similar results are obtained for M/L ratios in other optical passbands in combination with optical-optical colors.

The situation is slightly more complex when looking at trends in the K-band stellar M/L ratio with optical color (Fig. 2*c*). The age (as parameterized by τ) and metallicity

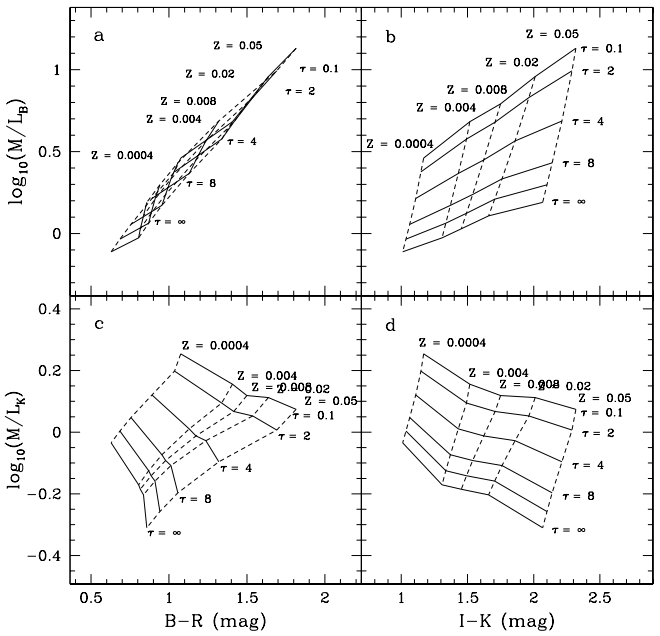

FIG. 2.—Trends in simple exponential SFH model stellar M/L ratios with color. Stellar M/L ratios for a Salpeter IMF in B (panels [*a*] and [*b*]) and K band (panels [*c*] and [*d*]) of single-metallicity exponentially declining star formation rate models from A. G. Bruzual & S. Charlot (2001, in preparation) are shown against the model $B-R$ (panels [*a*] and [*c*]) and $I-K$ (panels [*b*] and [*d*]) broadband colors. Models of the same e-folding timescale τ have been connected by solid lines, while models of the same metallicity Z are connected by dashed lines.

effects are no longer degenerate. However, realizing that chemical evolution caused by modest amounts of star formation raises the galaxy metallicity rapidly to at least 0.1 solar ($Z = 0.002$; in a closed box, conversion of $\sim 20\%$ of the gas mass into stars raises the average stellar metallicity to over 0.1 solar), the range of relevant metallicities becomes narrower, and the color-M/L correlation becomes tighter. Still, we expect a bit more scatter in the relations in the K band, in particular for very young galaxies with nearly primordial metallicities (like SBS 1415+437: with a metallicity of 0.05 solar it is one of the lowest metallicity galaxies known; Thuan, Izotov, & Foltz 1999).

We see that the method definitely breaks down when using $I-K$ versus M/L (Figs. 2*b* and 2*d*). This is because we are now using a color that is mainly a metallicity tracer versus M/L, which is more sensitive to age effects. We therefore expect the method to work best with optical-optical color combinations (which are unfortunately most affected by dust). Even though the K-band M/L-color relations are less tight, because of its much smaller dynamic range it is still the passband preferred for mass estimates, with I band providing a useful alternative.

4.2. *Stellar Population Model Uncertainties and IMFs*

In the above analysis we used the SPS models of A. G. Bruzual & S. Charlot (2001, in preparation) with a scaled-down Salpeter IMF, in conjunction with our own simple galaxy evolution models, to probe trends in stellar M/L ratio with galaxy properties. However, the SPS models carry with them their own sets of uncertainties, such as the prescriptions for post–main sequence evolution and the relationship between stellar properties and the observable colors. For this reason, we compare the stellar M/L ratios from a wide range of models here, to assess the robustness of our conclusions.

To test the consistency of the different SPS models (and later, the effect of different IMFs), we constructed a sequence of single-metallicity exponential SFH models with a range of metallicities and exponential e-folding timescales. Then, for each SPS model, we compare the correlation between $B-R$ color and stellar M/L ratio in a variety of passbands.

We show the effect of different SPS models in Figure 3 and in Table 4 in the Appendix. We adopt a Salpeter IMF and show the color-M/L relation for solar metallicity τ models in the B band (*thin lines*) and K band (*thick lines*). We show four SPS models: A. G. Bruzual & S. Charlot (2001, in preparation; *solid lines*), Kodama & Arimoto (1997; *dotted lines*), J. Schulz, U. Fritze-von Alvensleben, & K. J. Fricke (2001, in preparation; *short-dashed lines*), and the updated PÉGASE models of M. Fioc & B. Rocca-Volmerange (2001, in preparation; *long-dashed lines*).

For all models we find very similar slopes and zero points for the color-M/L relation (to within 0.1 dex in M/L ratio; Fig. 3). This also holds true for other passband combinations and metallicities. The only exception to this result is the J. Schulz et al. (2001, in preparation) model, which has an unusually bright asymptotic giant branch that produces very red optical–near-IR colors for solar metallicity stellar populations. The solar metallicity J. Schulz et al. (2001, in preparation) model gives normal B-band stellar M/L ratios but very low K-band stellar M/L ratios, compared to the other solar metallicity models. Essentially, this means that the J. Schulz et al. (2001, in preparation) solar metallicity model $B-K$ colors are redder than the other SPS models to which we compare (and, indeed, most of the luminous spiral galaxies in our observational sample). This poses a problem, however, as at a given optical-optical color (e.g., $B-R$) the optical–near-IR colors (e.g., $B-K$) of the solar metallicity J. Schulz et al. (2001, in preparation) models are far too red to explain observed galaxy colors, whereas the other models do reproduce the observed colors. In order to match observed spiral galaxy optical-optical and optical–near-IR colors simultaneously, one-third solar metallicity J. Schulz et al. (2001, in preparation) models must be adopted. We plot these models in Figure 3: these models have stellar M/L ratios much closer to other models' solar metallicity stellar M/L ratios. This slight model mismatch is actually quite useful: it demonstrates that even with substantial model differences, the stellar M/L ratio at a given optical–near-IR color is robust to model differences.

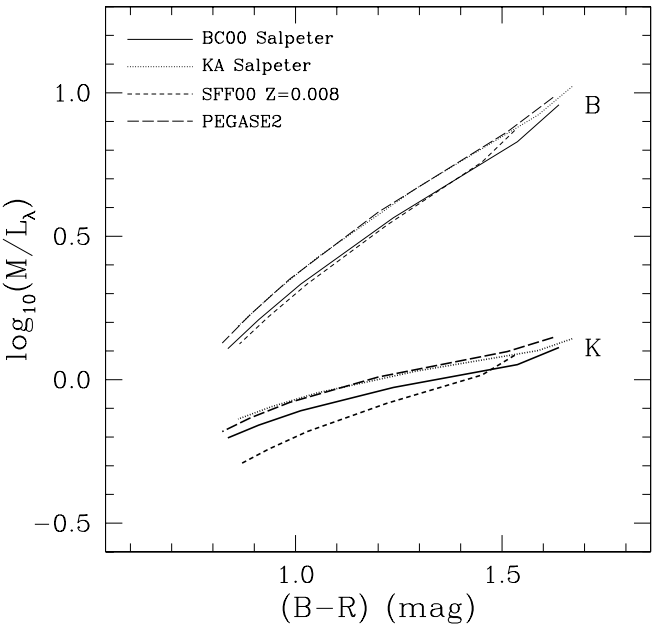

FIG. 3.—Comparison of the color-M/L relation for a sequence of exponentially declining star formation rate models of age 12 Gyr using a variety of SPS models. The red end of the lines represents a short burst of star formation, and the blue end represents a constant star formation rate model. The thin lines are for M/L_B, and the thicker lines are for M/L_K. The different models used are as follows: A. G. Bruzual & S. Charlot (2001, in preparation; *solid lines*), Kodama & Arimoto (1997; *dotted lines*), J. Schulz et al. (2001, in preparation; *dashed lines*), and updated PÉGASE models of M. Fioc & B. Rocca-Volmerange (2001, in preparation; *long-dashed lines*), all with a Salpeter IMF. All models have solar metallicity except for the J. Schulz et al. (2001, in preparation) models, which have one-third solar metallicity (see text for more details).

We now test the effect of different IMFs in Figure 4. We try out a wide range of IMFs for both the A. G. Bruzual & S. Charlot (2001, in preparation) and PÉGASE models: A. G. Bruzual & S. Charlot (2001, in preparation) models with a Salpeter IMF (with a logarithmic slope $x = -1.35$; *solid lines*), a Salpeter IMF modified to have a flat $x = 0$ slope below 0.6 $M_\odot$ (*dotted lines*), a Scalo (1986) IMF (*dashed lines*), and the updated PÉGASE models of M. Fioc & B. Rocca-Volmerange (2001, in preparation) with a steeper $x = -1.85$ IMF (*long-dashed lines*) and a flatter $x = -0.85$ IMF (*dot-dashed lines*). All models have solar metallicity. The slopes of the color-M/L correlations are independent of IMF: only the zero point is affected by the choice of IMF.

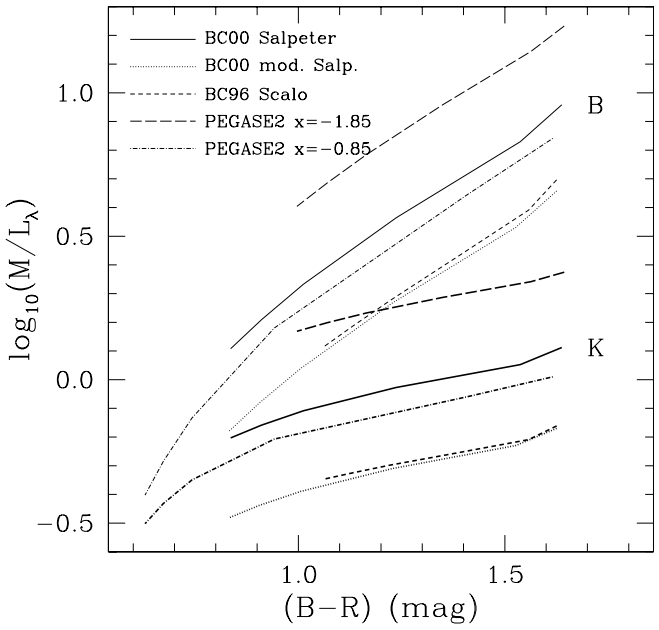

FIG. 4.—Comparison of the color-M/L relation for a sequence of exponentially declining star formation rate models of age 12 Gyr using a variety of IMFs. Again, the thin lines are for M/L_B, and the thicker lines are for M/L_K. The different models and IMFs used are as follows: A. G. Bruzual & S. Charlot (2001, in preparation) models with a Salpeter $x = -1.35$ IMF (*solid lines*), a Salpeter IMF with $x = 0$ below 0.6 $M_\odot$ (*dotted lines*), a Scalo (1986) IMF (*dashed lines*), and the updated PÉGASE models of M. Fioc & B. Rocca-Volmerange (2001, in preparation) with a steeper $x = -1.85$ IMF (*long-dashed lines*) and a flatter $x = -0.85$ IMF (*dot-dashed lines*). All models have solar metallicity.

The color range is also slightly affected by the IMF choice (especially the upper end of the IMF), as the range in models is from a single burst at the red end to constant star formation rate for 12 Gyr at the blue end. The sensitivity of the zero point of the color-M/L correlation to the IMF is due entirely to differences in the numbers of low-mass stars in each IMF. These low-mass stars significantly change the total mass of the stellar population but hardly change the overall color and luminosity of the system (which is dominated by the more massive stars). This justifies the scaling of the Salpeter IMF that we have done to bring the stellar M/L ratios of the Salpeter IMF into line with the maximum disk constraints in § 5: this scaling has the same effect as a flattening of the low-mass end of the IMF.

We therefore conclude that our choice of SPS model does not significantly affect our conclusions: in particular, the *relative* trend in stellar M/L ratio with color is preserved in all of the models that we examined. However, the model IMF does make a significant difference: while the IMF leaves the slope of the color-M/L correlation and the colors relatively unaffected, the IMF strongly affects the overall normalization of the stellar M/L ratio.

4.3. *Galaxy Evolution Uncertainties*

In this section we examine the uncertainties stemming from differences in galaxy evolution prescriptions. We have already examined the properties of six different galaxy evolution models in § 3 and the Appendix. We found that there was little difference between the behaviors of the closed-box, infall, outflow, dynamical time, mass-dependent formation epoch, and mass-dependent formation epoch with bursts models. In particular, the trends in stellar M/L ratio with color, and their zero points, were remarkably robust to a variety of different effects, including low-level bursts in the SFH. In addition, we have tested the effects of changing the age of galaxies at the present day from 12 Gyr: age changes of ± 3 Gyr produce changes in model stellar M/L ratio at a given color of only ± 0.05 dex.

One important issue is the effects of larger bursts: do galaxies with a recent or ongoing burst of star formation have stellar M/L ratios that vary considerably from the stellar M/L ratios of galaxies with more quiescent star formation but the same colors? We tested this case by adding a starburst with 0.5 Gyr duration to a range of exponential SFH models with a mass fraction of 10% of the total stellar mass formed over the lifetime of the galaxy. We viewed these models at a range of times after the burst, between 1 and 6 Gyr. A number of points are apparent from inspection of Figure 5. First of all, the effects of a 10% burst of star formation are much larger for red earlier type galaxies than for blue later type galaxies. This stems from the larger fractional contribution of the young stars to the total *luminosity* in redder galaxies. Secondly, maximum offsets from the color–stellar M/L ratio correlation are expected to be ~ 0.5 dex in B band and ~ 0.3 dex in K band. Thirdly, bursts of star formation bias the stellar M/L ratio to lower values at a given color. Finally, large effects are only visible for a period of ~ 1 Gyr for bluer underlying stellar populations but are visible for much longer (~ 5 Gyr) for redder underlying stellar populations.

This at first sight seems discouraging: in particular, the sensitivity of the stellar M/L ratio of redder underlying populations to a burst of star formation several gigayears ago implies significant scatter in the stellar M/L ratios of redder galaxies. This is part of our motivation for choosing a model with bursts of star formation as our default: with a model that incorporates bursts of star formation, we can account for the lower stellar M/L ratios of redder galaxies with even modest amounts of bursty star formation several gigayears ago (cf. Figs. 10*c* and 10*d* in the Appendix). However, we can take some comfort from the fact that our use of a 10% burst is very conservative: recent bursts of star formation that large are unlikely and are likely to be selected against in sample selection (by, e.g., selecting for undisturbed and symmetric galaxies). Indeed, even if morphological selection does not filter out these galaxies, galaxies with such large bursts are expected to lie off of the T-F relation (because their luminosities will have been considerably boosted by the starburst) and so may be selected against for this reason.

As a check, we have also examined the trends in stellar M/L ratio with color using disk-dominated nonsatellite galaxies from the hierarchical models of Cole et al. (2000). These models include the effects of halo formation and merging, gas cooling, star formation, feedback, and dust (but use the same SPS models as we adopt for this paper, with a Kennicutt 1983 IMF and a 38% brown dwarf fraction) and therefore offer a completely independent assessment of the effects of galaxy evolution prescriptions on the stellar M/L ratios of galaxies. The trend in their disk galaxy model stellar M/L ratios with color is almost identical to those of the simpler models (in particular, to the mass-dependent formation epoch with bursts model), albeit with more scatter due to the strongly irregular SFH (Fig. 10*f* of the Appendix). The key to the relatively modest scatter in model stellar M/L ratio with color in their models

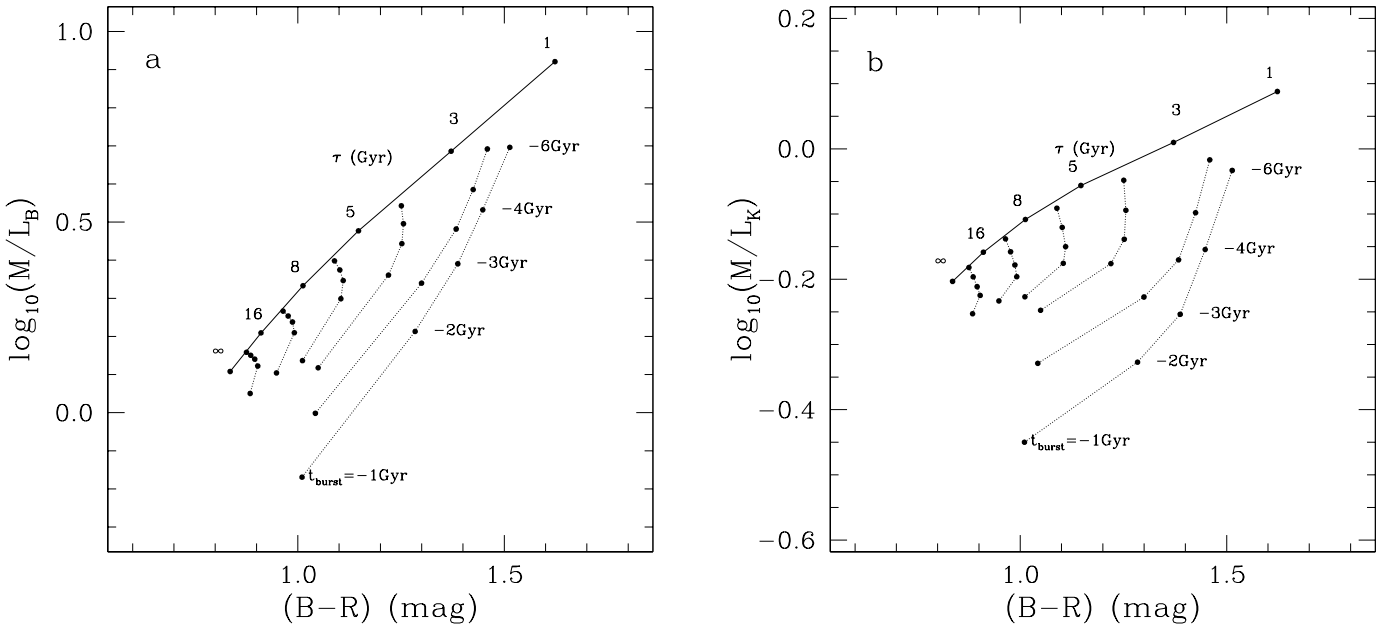

FIG. 5.—Color-M/L relations in (*a*) B band and (*b*) K band for a sequence of exponentially declining star formation rate solar metallicity models of age 12 Gyr with 10% mass fraction added in 0.5 Gyr starbursts. The solid line connects the exponential SFH models with different e-folding timescales τ. The dotted lines connect models of the same τ value, but with added starbursts occurring 1, 2, 3, 4, or 6 Gyr ago.

can be linked to the morphological transformations that accompany large mergers. Mergers large enough to produce large starbursts with large decreases in stellar M/L ratio are large enough to transform a disk-dominated galaxy into a spheroidal galaxy: these galaxies would not be included in any disk-dominated sample of galaxies.

We therefore conclude that choosing a different galaxy evolution prescription would not significantly affect the trends in model stellar M/L ratio with color presented in this paper. Large bursts of recent star formation can lower the stellar M/L ratio at a given color by up to a factor of 3; however, galaxies with a large amount of recent star formation are unlikely to feature heavily in a spiral galaxy sample. The lower level bursts more typical of disk-dominated spiral galaxies add only modest amounts of scatter to the color–stellar M/L ratio correlation and are accounted for by our default model.

4.4. *Dust*

Another potential concern is dust: dust simultaneously reddens and dims a stellar population, changing both axes in the correlation between color and stellar M/L ratio. We address this problem in Figure 1*d*, where we show dust extinction vectors for the dust correction of Tully et al. (1998) in B and K band. Dust extinction vectors for screen and Triplex models (Disney, Davies, & Phillipps 1989) are similar in direction to this vector. The dust vector shown in Figure 1 represents a large effect: it is the correction to face-on suffered by a Milky Way–type galaxy viewed at an inclination angle of 80°. For most galaxies the effects of extinction will be much smaller. It is clear that dust is a second-order effect for estimating stellar M/L ratios in this way. Dust extinguishes light from the stellar population, making it dimmer. However, dust also reddens the stellar population, making it appear to have a somewhat larger stellar M/L ratio. To first order, these effects cancel out, leaving a dust-reddened galaxy on the same color–stellar M/L ratio correlation. There is a possibility of over-predicting (underpredicting) the stellar M/L ratio (thus the stellar mass) if not enough (too much) reddening correction is applied, as the reddening effect is larger than the extinction effect. However, even for the large extinction error illustrated here, the effect is of order 0.1–0.2 dex. This error is comparable to the errors from uncertainties in SPS modeling and galaxy evolution prescriptions. However, this may not apply on a pixel-to-pixel level: some small regions of spiral galaxies may be optically thick in the optical, which completely obscures the light without producing any extra reddening (e.g., Witt, Thronson, & Capuano 1992). Therefore, smaller scale applications of this color-based stellar M/L ratio technique must be wary of the effects of dust.

4.5. *Summary*

The color–stellar M/L ratio correlation is robust in a relative sense (both within a passband and between passbands), *provided there is no systematic change in IMF with galaxy type.* Model uncertainties, galaxy evolution prescription uncertainties, small bursts of star formation, and dust uncertainties are all of order 0.1–0.2 dex or less. Large bursts of recent star formation may produce quite a large effect, depending on when they happen and on the properties of the underlying older stellar population. However, large bursts are unlikely to be common (at least at the present day: at higher redshift this need not be the case; e.g., Brinchmann & Ellis 2000). The IMF remains the largest uncertainty: assuming no trend in IMF with galaxy type, the range of IMFs presented in the literature causes uncertainty in the absolute normalization of the stellar M/L ratios of at least a factor of 2. We address this normalization in the next section.

5. ROTATION CURVES AND THE NORMALIZATION OF THE STELLAR M/L RATIO

We demonstrated that the model color–stellar M/L ratio correlation is robust in a relative sense but has uncertain

overall normalization. For many applications, this is perfectly acceptable. For example, it is quite possible to investigate the *slope* of the stellar mass T-F relation, or to estimate the trend in stellar M/L ratio as a function of galaxy radius for rotation curve fitting, without knowing the absolute normalization of the overall stellar M/L ratio. However, for some applications, e.g., for understanding the slope of the *baryonic* T-F relation, or in constraining the shape of dark matter halos, it is important to understand both the relative trend of stellar M/L ratio with color and the absolute normalization. The previous section showed that the question of the absolute normalization of the stellar M/L ratio essentially boils down to one issue: the stellar IMF. To first order, the amount of stellar light produced by observationally plausible IMFs is rather similar; however, the slope of the IMF, especially at the low-mass end, changes the overall stellar mass considerably.

We cannot address this problem fully, short of counting all of the stars in spiral galaxies directly. However, we can provide some constraints. The rotation curves of spiral galaxies have contributions from the stellar mass, gas mass, and dark matter. The relative contributions of each are difficult to estimate directly. However, interesting constraints can be derived by assuming that the mass of the stellar disk makes the maximum possible contribution to the rotation velocity: this is the maximum disk hypothesis (e.g., van Albada & Sancisi 1986). Fitting a maximal stellar disk to a rotation curve provides the maximum possible stellar M/L ratio, thus providing a firm upper limit to the stellar M/L ratios that we have constructed in the model.

We have examined the K-band maximum disk stellar M/L ratios of the Ursa Major Cluster sample of Verheijen (1997), rescaled to the *HST* Key Project distance of 20.7 Mpc (Sakai et al. 2000) to place constraints on the normalization of the stellar M/L ratios. This value is consistent (bearing in mind $\gtrsim$10% systematic uncertainties) with the distance derived from a different analysis of the Cepheid-calibrated T-F relation (18.6 Mpc; Tully & Pierce 2000) and the brightness of a Type 1a supernova in NGC 3992, which was consistent with a distance of 24 ± 5 Mpc (Parodi et al. 2000). K band was adopted, as we have shown above that using the K band results in the most robust stellar M/L ratio estimation. We consider the maximum stellar M/L ratio given by either the pseudoisothermal or Hernquist halo fit. In Figure 6 we plot this K-band maximum disk stellar M/L ratio against the $B-R$ color of the galaxy, dereddened assuming dust extinction following Tully et al. (1998; see also § 6). These are the dynamical upper limits for the stellar M/L ratios of these galaxies, hence the upper limit signs.

NGC 4085 is highlighted: this nearly edge-on galaxy was observed with a beam the size of its minor axis diameter, resulting in the worst-case scenario for beam smearing (e.g., van den Bosch et al. 2000). Consequently, it has a poorly resolved rotation curve, which biases the maximum disk M/L ratio downward. We ignore the stellar M/L ratio estimate for NGC 4085 in the following discussion, although clearly a better resolved rotation curve would be useful.

The main point of this plot is that our SPS-based model stellar M/L ratios should be the same as or lower than all of the observed maximum disk stellar M/L ratios. We make the explicit assumption here that the lower envelope of the observed maximum disk stellar M/L ratios is the meaningful constraint (again, we neglect NGC 4085 because of beam smearing). Galaxies with maximum disk M/L ratios significantly above this envelope are interpreted as galaxies with significant dark matter within the optical radius of the galaxy: these galaxies are submaximal. This interpretation is supported by the surface brightnesses of the submaximal disks: they are all fairly low surface brightness. Low surface brightness galaxies are thought to have high maximum disk stellar M/L ratios because they are dark matter dominated even in their inner regions (e.g., Verheijen 1997; de Blok & McGaugh 1998).

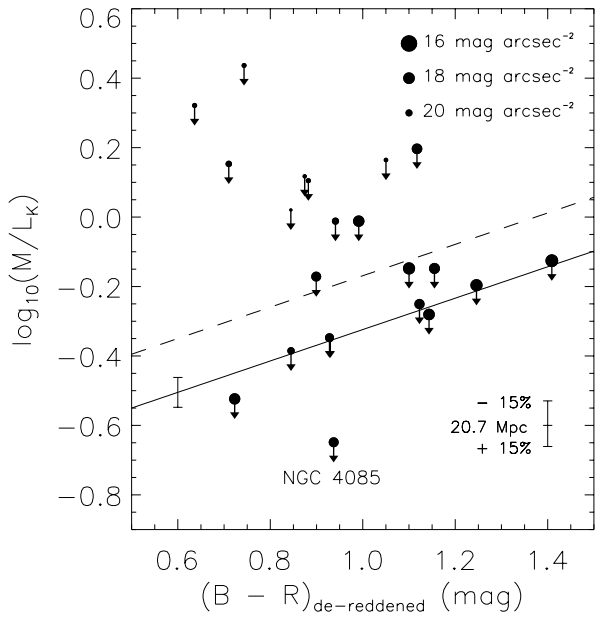

FIG. 6.—Observed K-band maximum disk stellar M/L ratios against dereddened $B-R$ color. The data are from K-band imaging and H I rotation curves from Verheijen (1997), rescaled to a distance of 20.7 Mpc (Sakai et al. 2000): the effect on the maximum disk M/L ratios of a $\pm$15% Ursa Major Cluster distance error is also shown. Overplotted is the least-squares fit to the correlation between color and stellar M/L ratio for the formation epoch with bursts model assuming a Salpeter (*dashed line*) and a scaled-down Salpeter IMF (*solid line*). We also show the rms spread of the formation epoch with bursts model around the color-M/L relation on the solid line as an error bar. NGC 4085 is highlighted: it has a poorly resolved rotation curve, which biases the maximum disk M/L ratio downward. Symbol size is coded by inclination-corrected K-band central surface brightness.

From Figure 6, it is clear that applying our standard color–stellar M/L ratio relation assuming a Salpeter $x = 1.35$ IMF normalization overpredicts the stellar M/L ratio of many of the galaxies (*dashed line*). Motivated by recent IMF determinations that suggest a turnover in the IMF at low stellar masses (e.g., Kroupa, Tout, & Gilmore 1993; Larson 1999; Kroupa 2000), we scale down the Salpeter IMF masses by a factor of 0.7. This is equivalent to a Salpeter IMF $x = 1.35$ with a flat $x = 0$ slope below 0.35 $M_\odot$, or a Kennicutt (1983) IMF with a brown dwarf fraction of $\sim$40%. This scaled IMF results in the solid line in Figure 6. This IMF is maximal: the stellar M/L ratios can be no larger than those predicted by a model adopting this IMF, modulo distance uncertainties. The maximum disk M/L ratios scale inversely with distance: a 15% error bar for the data points is shown, corresponding to a 10% random and 10% systematic error added in quadrature (Sakai et al. 2000). Indeed, the stellar M/L ratios might have to be even somewhat lower: all disks may be submaximal

(e.g., Bottema 1997; Courteau & Rix 1999), the K-band maximum disk stellar M/L ratio has not been corrected for the effects of dust extinction, and the mass locked up in molecular hydrogen has not been accounted for in these rotation curve decompositions. On the other hand, the H I rotation curves are all to some extent affected by at least small amounts of beam smearing (which would work to lower the maximum disk stellar M/L ratio estimate): the upshot is that there is some scope for moving the stellar M/L ratios only slightly upward, and there is much scope for moving the stellar M/L ratios substantially downward, lending credibility to the idea that our scaled Salpeter IMF is maximal.

One remarkable point is that, modulo the modest sample size, the slope of the lower envelope of the observational maximum disk stellar M/L ratios is accurately described by the predicted trend in K-band stellar M/L ratio with $B-R$ color. The zero point of the model has been constrained to match the data; however, there was no a priori reason that the slope of the observational color–stellar M/L ratio relation needed to match the predictions of the model. This is remarkable for a few reasons. First of all, it puts our proposition that the stellar M/L ratio is primarily a function of color, varying a factor of 2 in the K band between the reddest and bluest galaxies, on a more empirical footing. Secondly, it suggests that galaxies close to maximum disk have very similar IMFs, as strong IMF variations with galaxy color should be easily visible in this plot. In fact, the scatter of the observational lower envelope around the predicted line is consistent with the predicted model scatter due to differences in SFH at a given color, leaving *no* freedom for random galaxy-to-galaxy IMF variations. Finally, it implies that the galaxies closest to the observed limit (high surface brightness galaxies in general) are probably close to maximum disk because the adopted IMF already gives a reasonably low M/L ratio zero point, compared to other IMFs. At least the M/L ratios must be scaled to a relatively well defined maximum disk fraction (to better than $\lesssim 0.1$ dex, or 25%), which carries with it strong implications for scenarios of galaxy formation and evolution.

The above considerations have led to our preferred stellar M/L ratio model: we require that the model reproduces trends in color-based stellar ages and metallicities (Bell & Bower 2000; see also § 2), properly accounts for the decrease in the color–stellar M/L ratio slope caused by modest bursts of star formation (§ 4), and has an IMF consistent with maximum disk constraints (this section). These requirements are met by the mass-dependent formation epoch with bursts model, adopting a scaled Salpeter IMF (Fig. 1). We present least-squares fits to the color–stellar M/L ratio trend in Table 1. These fits can be used to estimate a stellar M/L ratio for a spiral galaxy stellar population of a given color, calibrated to maximum disk. If *all* (even very high surface brightness) galaxy disks are submaximal, the model fits should be scaled down by an appropriate, constant factor. The fits to our preferred model reproduce the color-M/L trends of the other models with this IMF to better than 0.1 dex (Fig. 10 and Table 3 in the Appendix). These fits are illustrated in Figure 1*d*, as well as in Figures 9 and 10 by the straight lines. The full models and fits of stellar M/L ratio against colors not considered in this paper are available from the authors. In particular, fits of the stellar M/L ratio with colors in the Sloan system will become available when the final bandpasses are defined.

6. THE TULLY-FISHER RELATION

Having established that galaxy evolution models make robust predictions of a correlation between optical colors and stellar M/L ratios, we will now investigate the implications for the T-F relation. The T-F relation relates the dynamical mass of a galaxy to its luminosity, thus providing a stringent test of theories of galaxy formation and evolution (e.g., Cole et al. 2000; Navarro & Steinmetz 2000b; van den Bosch 2000). However, its power as a test of theories is limited by its passband-dependent slope (this assumes linearity of the T-F relation, which seems a reasonable assumption over much of the T-F relation, although the T-F relation may be nonlinear at low galaxy masses; e.g., Matthews et al. 1998; McGaugh et al. 2000). The slope of the T-F relation varies from around $L \propto V^3$ in the blue to $L \propto V^4$ in the near-IR. Depending on to which passband a theory compares its T-F relation, it is possible to have a favorable comparison with one particular T-F relation but provide a poor match to a T-F relation at a different wavelength. There are, of course, more complex models that include realistic stellar population prescriptions and may be able to reproduce the T-F relations at many wavelengths (e.g., Heavens & Jimenez 1999; Cole et al. 2000); however, it would clearly be useful to be able to compare the models with one unique, passband-independent T-F relation.

In this section we apply the trends in stellar M/L ratio with spiral galaxy color described in Table 1 to the T-F relation data of Verheijen (1997) with a dual aim. First, we wish to test the stellar M/L ratios derived in § 3 to check if the stellar masses derived from different passbands give consistent results. Secondly, we wish to find out if there is a single, passband-independent T-F relation, and if so, what its slope is (assuming a linear T-F relation). The identification of a single, passband-independent T-F relation will allow even simplistic models to compare meaningfully with

TABLE 1

STELLAR M/L RATIO AS A FUNCTION OF COLOR FOR THE FORMATION EPOCH MODEL WITH BURSTS, ADOPTING A SCALED SALPETER IMF

Color	a_B	b_B	a_V	b_V	a_R	b_R	a_I	b_I	a_J	b_J	a_H	b_H	a_K	b_K
$B-V$	−0.994	1.804	−0.734	1.404	−0.660	1.222	−0.627	1.075	−0.621	0.794	−0.663	0.704	−0.692	0.652
$B-R$	−1.224	1.251	−0.916	0.976	−0.820	0.851	−0.768	0.748	−0.724	0.552	−0.754	0.489	−0.776	0.452
$V-I$	−1.919	2.214	−1.476	1.747	−1.314	1.528	−1.204	1.347	−1.040	0.987	−1.030	0.870	−1.027	0.800
$V-J$	−1.903	1.138	−1.477	0.905	−1.319	0.794	−1.209	0.700	−1.029	0.505	−1.014	0.442	−1.005	0.402
$V-H$	−2.181	0.978	−1.700	0.779	−1.515	0.684	−1.383	0.603	−1.151	0.434	−1.120	0.379	−1.100	0.345
$V-K$	−2.156	0.895	−1.683	0.714	−1.501	0.627	−1.370	0.553	−1.139	0.396	−1.108	0.346	−1.087	0.314

NOTE.—$\log_{10}(M/L) = a_\lambda + b_\lambda$ Color. Note that the stellar M/L values can be estimated for any combination of the above colors by a simple linear combination of the above fits. Note also that if *all* (even very high surface brightness) disks are submaximal, the above zero points should be modified by subtracting a constant from the above relations.

observations without having to construct a complex and realistic SFH model.

6.1. *The Data*

Here we use the T-F data obtained by Verheijen (1997) of the Ursa Major Cluster. The Ursa Major Cluster is a nearby (*HST* Key Project distance $D = 20.7$ Mpc; Sakai et al. 2000), poor cluster rich in spiral galaxies. The Verheijen data set is particularly suitable for our purposes because it provides accurate magnitudes in B, R, I, and K' and has accurate rotation velocities from well-resolved H I aperture synthesis rotation curves. We here consider only the rotation velocity at the flat part of the rotation curve ($v_{\rm flat}$): Verheijen (1997) concludes that use of this rotation velocity minimizes the scatter of the T-F relation. Furthermore, the rotation velocity at the flat part of the rotation curve is a "clean" observational quantity at a reasonably well defined radial range. The H I line width is a much more ill-defined quantity, resulting from the interplay of the rotation curve and global H I distribution (even neglecting the influence of warps, asymmetries, kinematic irregularities, and gaseous velocity dispersion). Thus, while the use of line width–based T-F relations for distance estimation purposes is perfectly valid, the use of line widths for constructing the *intrinsic* T-F relation as a test of galaxy evolution models is far from ideal. Using $v_{\rm flat}$ is much fairer and better reflects the true relationship between the rotation velocity of a galaxy and the stellar populations in that galaxy.

We correct for foreground galactic extinction assuming a B-band extinction of 0.08 mag (Schlegel, Finkbeiner, & Davis 1998). We further correct for extinction internal to the galaxy following Tully et al. (1998), who determined a galaxy line width–dependent extinction correction by minimizing scatter around the color-magnitude and T-F relations for a sample of 87 galaxies (although the Ursa Major Cluster galaxies form part of the data set defining the dust correction, meaning that the dust correction we use was partially derived from the T-F relation data we analyze here). According to this recipe, high-mass galaxies have a significant extinction correction, whereas low-mass galaxies have a negligible extinction correction. We adopt the line width–dependent version of this correction. Independent support for a mass-dependent extinction correction comes from de Jong & Lacey (2000), who use a sample of nearly 1000 spiral galaxies to find that high surface brightness (usually luminous) galaxies have optical depths of the order of 1 in their center, but that low surface brightness (usually less luminous) galaxies behave in a nearly transparent manner. For reference, we also tried the mass-independent extinction correction applied by Verheijen (1997) based on the method of Tully & Fouqué (1985).

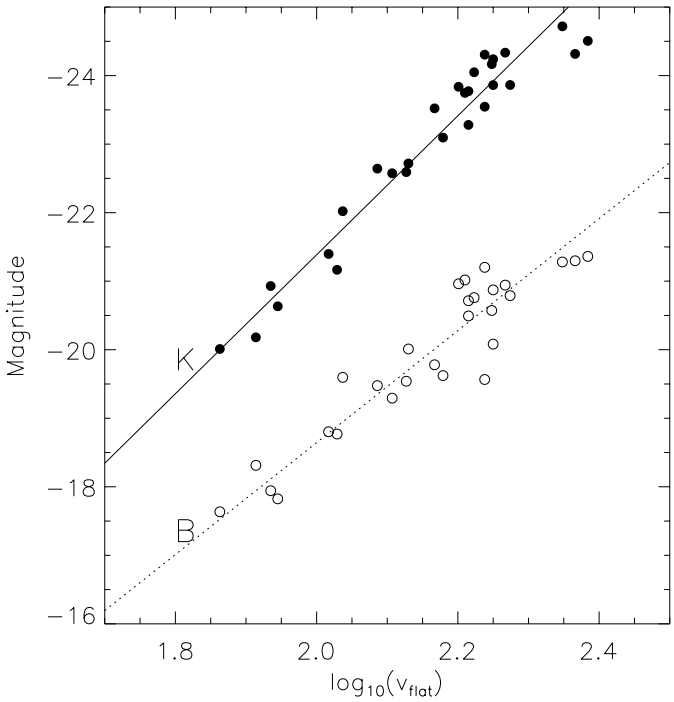

FIG. 7.—T-F relation in B and K passbands. Solid and open circles denote the data of Verheijen (1997) in K and B bands, respectively, corrected using the Tully et al. (1998) mass-dependent dust corrections. The lines denote the least-squares bisector fits (Isobe et al. 1990) to the mass-dependent dust-corrected T-F relations.

The T-F relations in B and K bands are shown in Figure 7, as are the best-fit least-squares bisectors (see also Table 2). Least-squares bisectors (Isobe et al. 1990) are the average of the "forward" and "backward" fits to the T-F relation (which have shallower and steeper slopes than this fit, respectively) and are particularly suitable for probing the intrinsic correlation between two variables. From Table 2 and Figure 7, it is immediately apparent that the T-F rela-

TABLE 2

INTERCEPTS AND SLOPES OF THE T-F RELATIONS: $L = L_{100}V^{\alpha}$ AND $M = M_{100}V^{\alpha}$

	B		R		I		K	
Case	$\log_{10} L_{100}/L_{\odot}$	α	$\log_{10} L_{100}/L_{\odot}$	α	$\log_{10} L_{100}/L_{\odot}$	α	$\log_{10} L_{100}/L_{\odot}$	α
Luminosities								
Mass-dep. dust	9.65 ± 0.03	3.27 ± 0.17	9.60 ± 0.03	3.54 ± 0.16	9.62 ± 0.03	3.77 ± 0.17	9.89 ± 0.03	4.06 ± 0.20
Mass-indep. dust	9.84 ± 0.03	2.76 ± 0.15	9.69 ± 0.03	3.18 ± 0.15	9.68 ± 0.03	3.46 ± 0.17	9.88 ± 0.03	3.98 ± 0.20
Masses								
Stellar mass (MD).....	9.51 ± 0.04	4.34 ± 0.22	9.51 ± 0.04	4.34 ± 0.22	9.49 ± 0.04	4.49 ± 0.23	9.49 ± 0.04	4.51 ± 0.26
Stellar mass (MI).....	9.38 ± 0.04	4.33 ± 0.23	9.38 ± 0.04	4.33 ± 0.23	9.35 ± 0.04	4.49 ± 0.24	9.37 ± 0.04	4.62 ± 0.25
Baryonic mass (MD).....	9.79 ± 0.04	3.45 ± 0.18	9.79 ± 0.04	3.45 ± 0.18	9.78 ± 0.04	3.55 ± 0.19	9.79 ± 0.04	3.51 ± 0.19

NOTE.—$L_{100}/L_{\odot}$ and $M_{100}/M_{\odot}$ are luminosities and masses in solar units for a galaxy on the T-F relation with a $v_{\rm flat}$ of 100 km s^{-1}. Case (MI) uses Tully & Fouqué 1985 mass-independent dust corrections, and case (MD) uses Tully et al. 1998 mass-dependent dust corrections. Errors denote the uncertainty in the formal fit to the T-F relations.

tion is shallower in the bluer passbands than in the near-IR, even accounting for magnitude-dependent dust corrections (e.g., Verheijen 1997; Tully et al. 1998). Furthermore, the T-F relation constructed using mass-independent dust corrections is shallower than the T-F relation constructed using the mass-dependent dust corrections of Tully et al. (1998): the discrepancy worsens as the passband becomes bluer. The fact that the T-F relation steepens at longer wavelengths, even when accounting for mass-dependent dust corrections, is a clear indication that the stellar M/L ratio varies with mass in just the way implied by Figure 1.

6.2. *The Stellar Mass T-F Relation*

To test this possibility in more detail, we adopt the least-squares fit to the variation of stellar M/L ratio with $B-R$ color in B, R, I, and K passbands for the preferred model (formation epoch model with bursts, with a scaled Salpeter IMF). These model relations are used to convert the magnitude-dependent dust-corrected magnitudes into stellar masses, using the dust-corrected $B-R$ color as input. The use of these model relations is suitable: the T-F relation from Verheijen (1997) is among the tightest in the literature, implying a minimal contribution from large starbursts. The results are shown in Figure 8*a*. Stellar masses derived from B and R passbands are shown as open circles (the masses are identical as the $B-R$ color was used to construct the M/L ratios), the I band as crosses, and the K band as filled circles. Least-squares bisector fits of the T-F relations are also shown and given in Table 2.

From Figure 8*a* and Table 2, it is clear that by accounting for the variation in stellar M/L ratio with galaxy color we have demonstrated that there is one passband-independent stellar mass T-F relation. The stellar masses determined from $B+R$-, I-, and K-band data for the individual galaxies are consistent to within $\sim 10\%$ rms, powerfully demonstrating the utility of this technique and confirming that the trends suggested by our models are indeed consistent with observations. Furthermore, the stellar mass T-F relation ($L \propto V^{4.4\pm0.2}$) is steeper than even the K-band T-F relation ($L \propto V^{4\pm0.2}$). These errors represent only fitting error: errors in IMF and distance scale do not affect the slope of the stellar mass T-F relation, and slope errors from adopting fits for different SFH models are ~ 0.2. In addition, the zero point of the stellar mass T-F relation is proportional to the distance, as we scale to maximum disk (a $\pm 15\%$ distance uncertainty translates into a ± 0.06 dex zero-point shift in the stellar mass T-F relation).

The scatter in the stellar mass T-F relation is somewhat less than 0.5 mag, which is slightly larger than the scatter in the *raw* optical and near-IR T-F relations. This is an unavoidable disadvantage of this technique: not only are we making the T-F relation steeper (which increases the magnitude scatter if some of the scatter is caused by velocity or distance errors), but we are folding uncertainties from at least two different passbands' data into the stellar T-F relation. However, a slightly enhanced scatter is a relatively modest price to pay: the true strength of this type of analysis is in the recovery of a stellar and/or baryonic mass T-F relation that is passband independent.

An interesting test is to consider the effects of the dust correction on the recovered stellar mass T-F relation. For example, even assuming that the dust correction of Tully et al. (1998) is appropriate statistically, the dust correction is unlikely to be accurate on a case-by-case basis. Thus, it is important to test the effects of choosing a different attenuation for the galaxy. We do this by repeating the above analysis using the mass-independent dust-corrected T-F relation (Verheijen 1997), the results of which are shown in Figure 8*b* and Table 2. Comparing the results in Table 2, we confirm the conclusion drawn about reddening in § 4.4: the stellar mass T-F estimated using a mass-independent dust prescription is almost exactly the same as the mass-dependent dust case. A modest offset of -0.13 dex is found, which stems from a larger blue optical depth in Tully & Fouqué (1985) compared to Tully et al. (1998): this produces bluer dereddened $B-R$ colors, which lead to an overall offset in stellar mass T-F relation without a change in slope. One interesting implication of this finding is that we cannot say how much of the decreasing slope of the T-F relation with decreasing wavelength is due to dust and how much is due to stellar M/L ratio differences. We expect the effects to be roughly comparable, as the Tully et al. (1998) corrections seem, at least in a statistical sense, quite appropriate.

6.3. *The Baryonic Mass T-F Relation*

When we account for the H I gas fraction to calculate the total known baryon mass (Fig. 8*c*), we find $m_{\rm baryon} \propto V^{3.5\pm0.2}$ (using an unweighted least-squares bisector fit). Since the baryonic T-F relation is of significant astro-

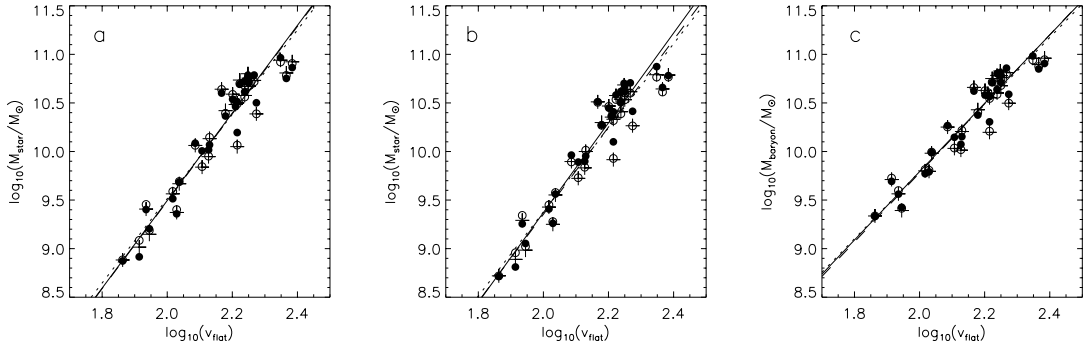

FIG. 8.—T-F relations: (*a*) stellar mass with mass-dependent extinction correction, (*b*) stellar mass with mass-independent extinction correction, and (*c*) baryonic T-F relation with mass-dependent extinction correction. Masses derived from B and R data are shown as open circles (the masses are identical as $B-R$ colors are used to construct the stellar M/L ratios), I-band data as crosses, and K-band data as solid circles. Least-squares bisector fits to each passband's T-F relations are presented for the B and R data (*dotted lines*), I-band data (*dashed lines*), and K-band data (*solid lines*).

physical importance, it is worth discussing the uncertainties in the slope we determine above. We have used an unweighted least-squares bisector: the slopes of forward and backward fits are ~ 0.15 shallower and steeper, respectively. There is an uncertainty of ± 0.2 or so depending on which model is used as the preferred model. Furthermore, we have not accounted for the (fairly unconstrained) molecular hydrogen mass fraction: if molecular hydrogen were included, it would probably steepen the baryonic T-F relation slightly (Young & Knezek 1989). On the other hand, the absolute normalization of the stellar M/L ratio is maximal, which implies that the slope stated above is as steep as is allowed by maximum disk: for reference, adopting a 63% velocity (40% mass) maximal disk following Bottema (1997) or Courteau & Rix (1999) would make the baryonic T-F relation slope shallower by 0.5. Also, we have assumed the *HST* Key Project distance to the Ursa Major Cluster (Sakai et al. 2000). The stellar masses are proportional to distance because we scale to maximum disk; however, the H I masses are affected by the distance D^2. Sakai et al. (2000) estimate around 10% random and 10% systematic distance uncertainties: the corresponding $\pm 15\%$ total distance error bars lead to slope changes of somewhat less than ∓ 0.1. This suggests that the random and systematic errors for the baryonic T-F relation slope should be ~ 0.2 each.

It should be noted that the scatter in the baryonic and stellar mass T-F relations can place tight constraints on the allowed variations in IMF at a given rotation velocity. The scatter in the baryonic T-F relation is a modest 0.1 dex, and in the stellar mass T-F relation it is a slightly larger 0.13 dex. Assuming that *all* of the error is due to IMF variations, a FWHM spread of stellar M/L ratios of somewhat less than a factor of 2 is allowed at a given rotation velocity. This is a firm upper limit as we do not account for measurement errors in the luminosity, rotation velocity, the intrinsic depth of the cluster, noncircular potentials (Franx & de Zeeuw 1992), or the intrinsic spread in stellar M/L ratios from SFH variations. Taken together with the suggestive tightness of the lower envelope of observational maximum disk stellar M/L ratios in Figure 6, which argues against large IMF variations at a given color, there is little evidence against a universal spiral galaxy IMF.

One interesting comparison that we can perform is with the baryonic T-F relation of McGaugh et al. (2000). They use a constant stellar M/L ratio in each passband to construct a baryonic T-F relation with a slope that is indistinguishable from 4. They claim that this strongly rules out cold dark matter–like models. We disagree with their result for the slope by around 2 σ (even including systematic error): adopting our slope of 3.5 ± 0.2 (random) ± 0.2 (systematic), the case against the basic relationship $m \propto V_{\rm halo}^3$ predicted by simple cold dark matter models is much weaker (e.g., van den Bosch 2000; Navarro & Steinmetz 2000b).

This disagreement is at first sight somewhat surprising, as accounting for the larger stellar M/L ratios and dust extinctions of redder galaxies would steepen the baryonic T-F relation, relative to one constructed assuming color-independent stellar M/L ratios and dust correction. However, the difference can be traced to a combination of three effects. First, and most importantly, McGaugh et al. (2000) use values of stellar M/L ratio that are around 30%–40% larger than ours (at a typical color for a luminous spiral galaxy) and assume a distance 25% shorter than the one we adopt. This accounts for most of the difference in baryonic T-F relation slope. Secondly, McGaugh et al. (2000) use line widths to construct their baryonic T-F relation. For a variety of reasons outlined earlier, we chose to use the more physically motivated rotation velocities at the flat part of the rotation curve: this leads to a shallower T-F relation by perhaps as much as 0.2 in terms of the slope (Verheijen 1997, Table 7). Finally, we lack galaxies with rotation velocities much lower than 80 km s^{-1}: at present, there is no sample of low-mass galaxies with sufficiently accurate rotation velocities and photometry to construct accurate $v_{\rm flat}$ and stellar mass estimates. The inclusion of low-mass galaxies may steepen the T-F relation or indicate that at low masses the T-F relation is nonlinear (e.g., Matthews et al. 1998).

7. CONCLUSIONS

Under the assumption of a universal spiral galaxy IMF, we have used SPS models in conjunction with simplified spiral galaxy evolution models to argue that there are substantial variations in stellar M/L ratio in optical and near-IR passbands and that these M/L ratio variations are strongly correlated with stellar population colors. The variations in stellar M/L ratio also correlate with other galaxy properties (albeit with more scatter) such that, on average, low surface brightness, high gas fraction, and low-luminosity galaxies have lower stellar M/L ratios than high surface brightness, low gas fraction, bright galaxies. The changes in stellar M/L ratios over a plausible range of galaxy parameters amount to a factor of about 7 in B, 3 in I, and 2 in K band. In addition, because the central regions of galaxies are often redder than their outer regions, the inner regions of galaxies are likely to have larger stellar M/L ratios than the outer regions of galaxies.

This strong correlation between color and stellar M/L ratio is robust to uncertainties in stellar population and galaxy evolution modeling, including the effects of modest bursts of recent star formation. Larger bursts, which are correspondingly more rare and are typically selected against in spiral galaxy studies (as evidenced by the modest scatter in our T-F relation), may depress the stellar M/L ratio from our expectations by up to 0.5 dex, at most. In addition, because dust both dims and reddens the light from galaxies, uncertainties in the exact amount of dust do not significantly affect the stellar mass estimate for a given galaxy. The stellar IMF remains the primary uncertainty, implying that these trends are relative in a robust sense, but the absolute normalization is somewhat uncertain.

We analyzed observed K-band maximum disk stellar M/L ratios from Verheijen (1997) to place the relative stellar M/L ratios that we estimate in this paper on the maximum allowed scale. We find that a Salpeter IMF is ruled out by this analysis if the Ursa Major Cluster is placed at the *HST* Key Project distance of 20.7 Mpc and that modification of the low-mass end of the IMF is required. We find that the observed maximum disk stellar M/L ratios follow the trend suggested by the models, which lends independent support for our models, implies that a fraction of high surface brightness galaxies are reasonably close to maximum disk, and suggests a universal spiral galaxy stellar IMF.

We apply these maximum disk–scaled trends in stellar M/L ratio with galaxy color to investigate the underlying nature of the T-F relation. We find that, using mass-

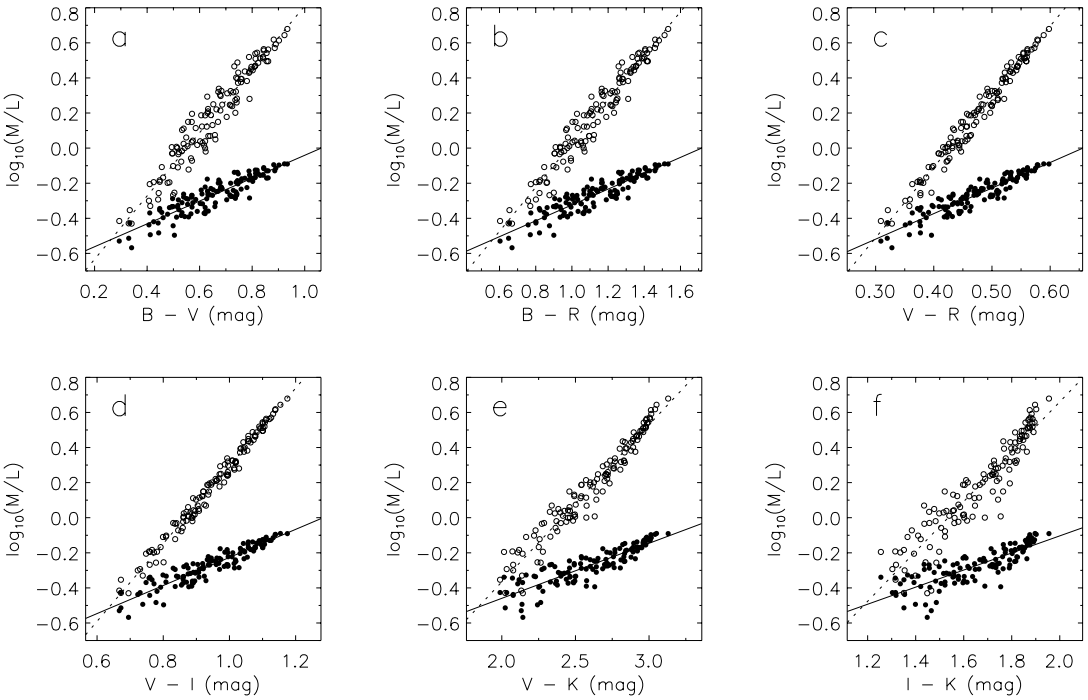

FIG. 9.—Trends in stellar M/L for the formation epoch model with bursts in K (*filled circles*) and B band (*open circles*) with (*a*) $B-V$, (*b*) $B-R$, (*c*) $V-R$, (*d*) $V-I$, (*e*) $V-K$, and (*f*) $I-K$ color. We also show the least-squares fit to the variations of stellar M/L ratio with color for the B-band (*dotted line*) and K-band (*solid line*) stellar M/L ratio.

dependent dust extinction corrections and the color-dependent stellar M/L ratios, it is possible to estimate stellar masses from different passbands that are consistent at better than the 10% level. The slope of the stellar mass T-F relation of the Ursa Major Cluster sample is 4.4 ± 0.2, using a least-squares bisector fit. Including the contribution from the H I mass, we find that the slope of the baryonic T-F relation of the Ursa Major Cluster is 3.5 ± 0.2

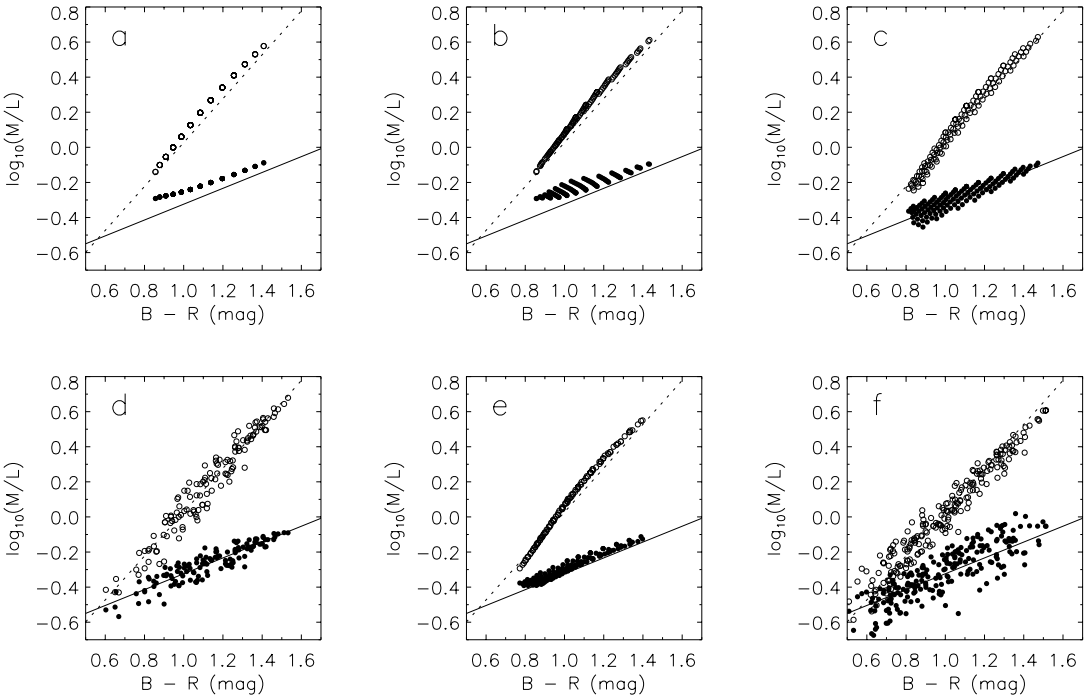

FIG. 10.—Trends in stellar M/L with $B-R$ color for six different galaxy evolution models in K (*filled circles*) and B band (*open circles*) for the (*a*) closed-box model, (*b*) outflow model, (*c*) mass-dependent formation epoch model, (*d*) mass-dependent formation epoch model with bursts, (*e*) infall model, and (*f*) Cole et al. (2000) hierarchical model. We also show the least-squares fit to the variations of stellar M/L ratio with $B-R$ color of the mass-dependent formation epoch with bursts model for the B (*dotted line*) and K band (*solid line*). The Cole et al. (2000) model adopts a Kennicutt (1983) IMF and a 38% brown dwarf fraction, which results in a similar zero point to the scaled-down Salpeter IMF we adopt.

TABLE 3

STELLAR M/L RATIO AS A FUNCTION OF COLOR FOR THE SCALED SALPETER IMF

Model	a_B	b_B	a_V	b_V	a_R	b_R	a_I	b_I	a_J	b_J	a_H	b_H	a_K	b_K
							$B-V$							
Closed box	−1.019	1.937	−0.759	1.537	−0.681	1.346	−0.631	1.170	−0.540	0.767	−0.553	0.632	−0.554	0.540
Infall	−1.113	2.065	−0.853	1.665	−0.772	1.468	−0.723	1.290	−0.658	0.907	−0.679	0.777	−0.692	0.699
Outflow	−1.026	1.954	−0.766	1.554	−0.685	1.357	−0.634	1.179	−0.527	0.741	−0.536	0.600	−0.534	0.500
Dynamical time	−0.990	1.883	−0.730	1.483	−0.650	1.289	−0.601	1.114	−0.514	0.704	−0.528	0.569	−0.531	0.476
Formation epoch	−1.110	2.018	−0.850	1.618	−0.770	1.425	−0.724	1.257	−0.659	0.878	−0.683	0.757	−0.694	0.676
Formation epoch: bursts	−0.994	1.804	−0.734	1.404	−0.660	1.222	−0.627	1.075	−0.621	0.794	−0.663	0.704	−0.692	0.652
Cole et al. (2000)	−0.888	1.758	−0.628	1.358	−0.565	1.132	−0.525	0.981	−0.550	0.801	−0.618	0.718	−0.654	0.696
							$B-R$							
Closed box	−1.236	1.312	−0.932	1.042	−0.832	0.912	−0.762	0.793	−0.626	0.519	−0.623	0.427	−0.613	0.364
Infall	−1.334	1.386	−1.032	1.119	−0.930	0.986	−0.861	0.867	−0.754	0.608	−0.760	0.520	−0.764	0.467
Outflow	−1.236	1.313	−0.933	1.045	−0.832	0.913	−0.761	0.793	−0.604	0.496	−0.598	0.400	−0.583	0.332
Dynamical time	−1.195	1.270	−0.892	1.001	−0.791	0.870	−0.723	0.752	−0.590	0.474	−0.589	0.382	−0.581	0.319
Formation epoch	−1.333	1.365	−1.030	1.095	−0.929	0.965	−0.865	0.851	−0.757	0.594	−0.767	0.512	−0.769	0.457
Formation epoch: bursts	−1.224	1.251	−0.916	0.976	−0.820	0.851	−0.768	0.748	−0.724	0.552	−0.754	0.489	−0.776	0.452
Cole et al. (2000)	−1.121	1.130	−0.811	0.875	−0.717	0.730	−0.657	0.633	−0.657	0.516	−0.713	0.461	−0.746	0.447
							$V-I$							
Closed box	−1.771	2.104	−1.359	1.674	−1.207	1.466	−1.087	1.274	−0.835	0.830	−0.791	0.679	−0.755	0.578
Infall	−1.882	2.191	−1.478	1.772	−1.323	1.563	−1.206	1.372	−0.988	0.954	−0.955	0.810	−0.935	0.723
Outflow	−1.743	2.072	−1.341	1.653	−1.188	1.445	−1.069	1.253	−0.786	0.772	−0.737	0.615	−0.692	0.503
Dynamical time	−1.714	2.035	−1.304	1.607	−1.150	1.398	−1.032	1.207	−0.781	0.757	−0.739	0.606	−0.703	0.503
Formation epoch	−1.931	2.234	−1.513	1.797	−1.356	1.584	−1.241	1.397	−1.017	0.972	−0.989	0.835	−0.965	0.744
Formation epoch: bursts	−1.919	2.214	−1.476	1.747	−1.314	1.528	−1.204	1.347	−1.040	0.987	−1.030	0.870	−1.027	0.800
Cole et al. (2000)	−1.674	1.865	−1.249	1.456	−1.088	1.220	−0.977	1.056	−0.901	0.843	−0.924	0.745	−0.943	0.714
							$V-J$							
Closed box	−1.574	0.993	−1.204	0.791	−1.071	0.693	−0.969	0.602	−0.756	0.391	−0.725	0.319	−0.698	0.271
Infall	−1.740	1.054	−1.365	0.854	−1.224	0.753	−1.117	0.660	−0.917	0.454	−0.889	0.382	−0.872	0.338
Outflow	−1.453	0.920	−1.113	0.735	−0.989	0.643	−0.895	0.557	−0.665	0.335	−0.633	0.263	−0.599	0.211
Dynamical time	−1.524	0.952	−1.156	0.753	−1.022	0.655	−0.921	0.566	−0.708	0.353	−0.679	0.281	−0.651	0.232
Formation epoch	−1.780	1.072	−1.392	0.863	−1.250	0.761	−1.146	0.670	−0.944	0.463	−0.923	0.396	−0.903	0.350
Formation epoch: bursts	−1.903	1.138	−1.477	0.905	−1.319	0.794	−1.209	0.700	−1.029	0.505	−1.014	0.442	−1.005	0.402
Cole et al. (2000)	−1.854	1.141	−1.397	0.896	−1.215	0.752	−1.080	0.647	−0.949	0.496	−0.948	0.427	−0.953	0.402
							$V-H$							
Closed box	−1.782	0.840	−1.371	0.669	−1.217	0.586	−1.096	0.509	−0.838	0.330	−0.791	0.269	−0.753	0.228
Infall	−1.962	0.889	−1.546	0.721	−1.384	0.636	−1.257	0.557	−1.011	0.382	−0.966	0.321	−0.939	0.284
Outflow	−1.641	0.776	−1.264	0.621	−1.121	0.543	−1.009	0.470	−0.731	0.282	−0.684	0.221	−0.639	0.176
Dynamical time	−1.725	0.805	−1.317	0.638	−1.161	0.555	−1.042	0.479	−0.783	0.298	−0.737	0.238	−0.699	0.196
Formation epoch	−2.027	0.916	−1.592	0.737	−1.425	0.650	−1.300	0.572	−1.050	0.395	−1.012	0.337	−0.981	0.298
Formation epoch: bursts	−2.181	0.978	−1.700	0.779	−1.515	0.684	−1.383	0.603	−1.151	0.434	−1.120	0.379	−1.100	0.345
Cole et al. (2000)	−2.142	0.961	−1.627	0.756	−1.410	0.635	−1.246	0.546	−1.070	0.415	−1.047	0.356	−1.043	0.333
							$V-K$							
Closed box	−1.738	0.761	−1.336	0.607	−1.187	0.531	−1.069	0.462	−0.820	0.299	−0.776	0.244	−0.740	0.207
Infall	−1.931	0.811	−1.522	0.658	−1.363	0.580	−1.238	0.508	−0.996	0.348	−0.953	0.292	−0.926	0.258
Outflow	−1.583	0.696	−1.218	0.557	−1.081	0.487	−0.974	0.421	−0.708	0.252	−0.664	0.197	−0.622	0.157
Dynamical time	−1.682	0.728	−1.283	0.577	−1.132	0.502	−1.016	0.433	−0.766	0.270	−0.723	0.215	−0.687	0.177
Formation epoch	−1.990	0.832	−1.562	0.670	−1.399	0.590	−1.277	0.520	−1.032	0.358	−0.996	0.305	−0.966	0.270
Formation epoch: bursts	−2.156	0.895	−1.683	0.714	−1.501	0.627	−1.370	0.553	−1.139	0.396	−1.108	0.346	−1.087	0.314
Cole et al. (2000)	−2.125	0.891	−1.615	0.701	−1.400	0.590	−1.235	0.506	−1.051	0.380	−1.026	0.324	−1.019	0.301

NOTE.—$\log_{10}(M/L) = a_\lambda + b_\lambda$ Color. The Cole et al. 2000 model adopts a Kennicutt 1983 IMF and a 38% brown dwarf fraction, which results in a similar zero point to the scaled-down Salpeter IMF we adopt. Note that the stellar M/L values can be estimated for any combination of the above colors by a simple linear combination of the above fits. Table 3 is also available in machine-readable form in the electronic edition of the *Astrophysical Journal*.

TABLE 4

STELLAR M/L RATIO AS A FUNCTION OF COLOR FOR DIFFERENT SPS MODELS

Model	a_B	b_B	a_V	b_V	a_R	b_R	a_I	b_I	a_J	b_J	a_H	b_H	a_K	b_K
						$B-V$, $Z = 0.008$								
Bruzual & Charlot, Salpeter IMF	−0.63	1.54	−0.37	1.14	−0.30	0.97	−0.27	0.83	−0.33	0.68	−0.39	0.62	−0.43	0.60
Bruzual & Charlot, Scaled Salpeter IMF	−0.78	1.54	−0.52	1.14	−0.46	0.97	−0.43	0.83	−0.48	0.68	−0.54	0.62	−0.59	0.60
Bruzual & Charlot, Modified Salpeter IMF	−0.91	1.53	−0.65	1.13	−0.58	0.97	−0.56	0.84	−0.61	0.68	−0.67	0.61	−0.71	0.60
Bruzual & Charlot 96, Scalo IMF	−0.85	1.48	−0.59	1.08	−0.52	0.91	−0.49	0.79	−0.56	0.64	−0.63	0.57	−0.65	0.56
Kodama & Arimoto, Salpeter IMF	−0.56	1.46	−0.30	1.06	−0.24	0.91	−0.22	0.76	−0.26	0.61	−0.36	0.55	−0.38	0.53
Schulz et al., Salpeter IMF	−0.59	1.55	−0.33	1.15	−0.26	0.98	−0.29	0.86	−0.60	0.76	−0.51	0.75	−0.65	0.77
PÉGASE, Salpeter IMF	−0.57	1.51	−0.31	1.11	−0.24	0.95	−0.19	0.76	−0.25	0.65	−0.33	0.60	−0.38	0.59
PÉGASE, $x = -1.85$ IMF	−0.25	1.40	0.01	1.00	0.09	0.82	0.11	0.65	0.05	0.55	−0.03	0.49	−0.07	0.48
PÉGASE, $x = -0.85$ IMF	−0.87	1.75	−0.61	1.35	−0.56	1.20	−0.42	0.90	−0.47	0.79	−0.53	0.70	−0.59	0.71
						$B-V$, $Z = 0.02$								
Bruzual & Charlot, Salpeter IMF	−0.51	1.45	−0.25	1.05	−0.19	0.88	−0.17	0.76	−0.28	0.58	−0.36	0.53	−0.42	0.52
Bruzual & Charlot, Scaled Salpeter IMF	−0.66	1.45	−0.40	1.05	−0.34	0.88	−0.33	0.76	−0.43	0.58	−0.51	0.53	−0.57	0.52
Bruzual & Charlot, Modified Salpeter IMF	−0.79	1.43	−0.53	1.03	−0.47	0.87	−0.46	0.75	−0.55	0.58	−0.63	0.53	−0.69	0.51
Bruzual & Charlot 96, Scalo IMF	−0.74	1.40	−0.48	1.00	−0.42	0.84	−0.40	0.73	−0.49	0.51	−0.58	0.45	−0.61	0.43
Kodama & Arimoto, Salpeter IMF	−0.44	1.40	−0.18	1.00	−0.12	0.84	−0.12	0.70	−0.19	0.53	−0.30	0.48	−0.33	0.45
Schulz et al., Salpeter IMF	−0.49	1.46	−0.23	1.06	−0.16	0.89	−0.20	0.77	−0.59	0.61	−0.48	0.61	−0.64	0.62
PÉGASE, Salpeter IMF	−0.47	1.45	−0.21	1.05	−0.15	0.89	−0.12	0.71	−0.23	0.59	−0.34	0.55	−0.39	0.54
PÉGASE, $x = -1.85$ IMF	−0.15	1.36	0.11	0.96	0.18	0.79	0.19	0.62	0.09	0.49	−0.02	0.44	−0.07	0.44
PÉGASE, $x = -0.85$ IMF	−0.77	1.65	−0.51	1.25	−0.47	1.11	−0.35	0.85	−0.46	0.72	−0.55	0.65	−0.62	0.65
						$B-R$, $Z = 0.008$								
Bruzual & Charlot, Salpeter IMF	−0.84	1.08	−0.52	0.80	−0.43	0.68	−0.39	0.59	−0.42	0.48	−0.47	0.43	−0.51	0.42
Bruzual & Charlot, Scaled Salpeter IMF	−0.99	1.08	−0.68	0.80	−0.59	0.68	−0.54	0.59	−0.57	0.48	−0.63	0.43	−0.67	0.42
Bruzual & Charlot, Modified Salpeter IMF	−1.12	1.08	−0.81	0.80	−0.72	0.68	−0.68	0.59	−0.70	0.48	−0.75	0.44	−0.80	0.42
Bruzual & Charlot 96, Scalo IMF	−1.05	1.04	−0.74	0.76	−0.65	0.64	−0.60	0.56	−0.64	0.45	−0.70	0.40	−0.73	0.39
Kodama & Arimoto, Salpeter IMF	−0.77	1.05	−0.45	0.76	−0.36	0.65	−0.33	0.55	−0.35	0.44	−0.44	0.40	−0.45	0.38
Schulz et al., Salpeter IMF	−0.79	1.08	−0.48	0.80	−0.39	0.68	−0.40	0.60	−0.70	0.53	−0.61	0.52	−0.75	0.54
PÉGASE, Salpeter IMF	−0.78	1.08	−0.47	0.79	−0.38	0.68	−0.30	0.54	−0.35	0.46	−0.42	0.42	−0.47	0.42
PÉGASE, $x = -1.85$ IMF	−0.42	0.97	−0.11	0.70	−0.02	0.57	0.02	0.46	−0.02	0.38	−0.09	0.34	−0.13	0.33
PÉGASE, $x = -0.85$ IMF	−1.18	1.29	−0.85	0.99	−0.77	0.89	−0.58	0.66	−0.61	0.58	−0.65	0.52	−0.72	0.52
						$B-R$, $Z = 0.02$								
Bruzual & Charlot, Salpeter IMF	−0.73	1.03	−0.41	0.74	−0.32	0.63	−0.29	0.54	−0.36	0.41	−0.44	0.38	−0.49	0.37
Bruzual & Charlot, Scaled Salpeter IMF	−0.88	1.03	−0.56	0.74	−0.48	0.63	−0.44	0.54	−0.52	0.41	−0.59	0.38	−0.65	0.37
Bruzual & Charlot, Modified Salpeter IMF	−1.01	1.02	−0.69	0.74	−0.60	0.62	−0.57	0.54	−0.64	0.41	−0.71	0.38	−0.77	0.37
Bruzual & Charlot 96, Scalo IMF	−0.95	1.00	−0.63	0.71	−0.54	0.60	−0.50	0.52	−0.56	0.37	−0.65	0.32	−0.67	0.31
Kodama & Arimoto, Salpeter IMF	−0.65	1.00	−0.33	0.72	−0.25	0.60	−0.22	0.50	−0.27	0.38	−0.38	0.35	−0.40	0.32
Schulz et al., Salpeter IMF	−0.69	1.02	−0.38	0.74	−0.29	0.62	−0.31	0.54	−0.67	0.43	−0.57	0.43	−0.73	0.44
PÉGASE, Salpeter IMF	−0.70	1.04	−0.38	0.75	−0.29	0.64	−0.23	0.51	−0.32	0.43	−0.42	0.39	−0.48	0.39
PÉGASE, $x = -1.85$ IMF	−0.33	0.95	−0.02	0.67	0.07	0.55	0.10	0.44	0.02	0.34	−0.08	0.31	−0.13	0.31
PÉGASE, $x = -0.85$ IMF	−1.08	1.22	−0.74	0.92	−0.67	0.82	−0.51	0.62	−0.59	0.53	−0.67	0.48	−0.74	0.48

TABLE 4—*Continued*

Model	a_B	b_B	a_V	b_V	a_R	b_R	a_I	b_I	a_J	b_J	a_H	b_H	a_K	b_K
						$V-I$, $Z = 0.008$								
Bruzual & Charlot, Salpeter IMF	−1.53	2.01	−1.04	1.49	−0.87	1.27	−0.77	1.09	−0.73	0.88	−0.75	0.80	−0.78	0.78
Bruzual & Charlot, Scaled Salpeter IMF	−1.69	2.01	−1.19	1.49	−1.03	1.27	−0.92	1.09	−0.88	0.88	−0.91	0.80	−0.94	0.78
Bruzual & Charlot, Modified Salpeter IMF	−1.85	2.07	−1.34	1.53	−1.18	1.31	−1.07	1.13	−1.02	0.92	−1.05	0.83	−1.08	0.81
Bruzual & Charlot 96, Scalo IMF	−1.76	2.10	−1.25	1.53	−1.08	1.29	−0.98	1.13	−0.95	0.91	−0.98	0.81	−1.00	0.79
Kodama & Arimoto, Salpeter IMF	−1.49	1.95	−0.98	1.42	−0.81	1.21	−0.71	1.02	−0.65	0.81	−0.71	0.74	−0.71	0.70
Schulz et al., Salpeter IMF	−1.82	2.15	−1.25	1.60	−1.04	1.36	−0.98	1.20	−1.20	1.05	−1.10	1.03	−1.26	1.07
PÉGASE, Salpeter IMF	−1.25	1.70	−0.81	1.25	−0.67	1.07	−0.54	0.85	−0.55	0.74	−0.60	0.67	−0.65	0.67
PÉGASE, $x = -1.85$ IMF	−0.98	1.62	−0.51	1.16	−0.34	0.96	−0.24	0.76	−0.23	0.63	−0.29	0.57	−0.32	0.56
PÉGASE, $x = -0.85$ IMF	−1.18	1.57	−0.85	1.22	−0.78	1.09	−0.58	0.82	−0.61	0.71	−0.66	0.64	−0.72	0.64
						$V-I$, $Z = 0.02$								
Bruzual & Charlot, Salpeter IMF	−1.50	1.99	−0.97	1.44	−0.80	1.21	−0.70	1.04	−0.68	0.80	−0.72	0.73	−0.77	0.71
Bruzual & Charlot, Scaled Salpeter IMF	−1.65	1.99	−1.12	1.44	−0.95	1.21	−0.85	1.04	−0.83	0.80	−0.88	0.73	−0.93	0.71
Bruzual & Charlot, Modified Salpeter IMF	−1.81	2.04	−1.27	1.47	−1.09	1.24	−0.99	1.07	−0.97	0.83	−1.01	0.75	−1.06	0.73
Bruzual & Charlot 96, Scalo IMF	−1.71	2.06	−1.17	1.47	−1.00	1.24	−0.90	1.07	−0.84	0.75	−0.89	0.67	−0.91	0.63
Kodama & Arimoto, Salpeter IMF	−1.42	1.87	−0.88	1.34	−0.71	1.13	−0.61	0.94	−0.57	0.71	−0.64	0.65	−0.65	0.61
Schulz et al., Salpeter IMF	−1.73	2.02	−1.13	1.47	−0.92	1.23	−0.86	1.07	−1.11	0.84	−1.01	0.85	−1.18	0.86
PÉGASE, Salpeter IMF	−1.25	1.72	−0.78	1.25	−0.63	1.06	−0.50	0.85	−0.55	0.70	−0.63	0.65	−0.68	0.64
PÉGASE, $x = -1.85$ IMF	−0.93	1.61	−0.44	1.14	−0.28	0.93	−0.17	0.74	−0.20	0.58	−0.27	0.53	−0.32	0.52
PÉGASE, $x = -0.85$ IMF	−1.24	1.63	−0.87	1.24	−0.79	1.10	−0.60	0.84	−0.66	0.71	−0.74	0.65	−0.81	0.65
						$V-J$, $Z = 0.008$								
Bruzual & Charlot, Salpeter IMF	−1.98	1.32	−1.37	0.98	−1.15	0.84	−1.01	0.72	−0.92	0.58	−0.93	0.53	−0.96	0.51
Bruzual & Charlot, Scaled Salpeter IMF	−2.13	1.32	−1.52	0.98	−1.31	0.84	−1.16	0.72	−1.08	0.58	−1.08	0.53	−1.11	0.51
Bruzual & Charlot, Modified Salpeter IMF	−2.28	1.35	−1.66	1.00	−1.45	0.85	−1.31	0.74	−1.22	0.60	−1.22	0.54	−1.25	0.53
Bruzual & Charlot 96, Scalo IMF	−2.24	1.35	−1.60	0.98	−1.38	0.83	−1.24	0.73	−1.15	0.58	−1.16	0.52	−1.18	0.51
Kodama & Arimoto, Salpeter IMF	−1.87	1.29	−1.26	0.94	−1.05	0.80	−0.91	0.67	−0.81	0.54	−0.85	0.49	−0.85	0.46
Schulz et al., Salpeter IMF	−3.40	1.58	−2.42	1.17	−2.04	1.00	−1.86	0.88	−1.97	0.77	−1.86	0.76	−2.05	0.79
PÉGASE, Salpeter IMF	−1.86	1.31	−1.26	0.97	−1.06	0.83	−0.85	0.66	−0.82	0.57	−0.85	0.52	−0.89	0.51
PÉGASE, $x = -1.85$ IMF	−1.52	1.23	−0.89	0.88	−0.66	0.73	−0.49	0.58	−0.45	0.48	−0.48	0.43	−0.51	0.42
PÉGASE, $x = -0.85$ IMF	−1.82	1.24	−1.35	0.96	−1.23	0.86	−0.92	0.65	−0.90	0.56	−0.92	0.51	−0.99	0.51
						$V-J$, $Z = 0.02$								
Bruzual & Charlot, Salpeter IMF	−1.99	1.24	−1.32	0.90	−1.09	0.76	−0.95	0.65	−0.87	0.50	−0.90	0.46	−0.95	0.45
Bruzual & Charlot, Scaled Salpeter IMF	−2.14	1.24	−1.48	0.90	−1.25	0.76	−1.11	0.65	−1.03	0.50	−1.06	0.46	−1.10	0.45
Bruzual & Charlot, Modified Salpeter IMF	−2.29	1.27	−1.62	0.92	−1.39	0.77	−1.25	0.67	−1.17	0.52	−1.19	0.47	−1.23	0.46
Bruzual & Charlot 96, Scalo IMF	−2.04	1.15	−1.41	0.82	−1.20	0.69	−1.08	0.60	−0.97	0.42	−1.00	0.37	−1.01	0.35
Kodama & Arimoto, Salpeter IMF	−1.82	1.20	−1.17	0.86	−0.95	0.72	−0.81	0.60	−0.72	0.46	−0.78	0.41	−0.78	0.39
Schulz et al., Salpeter IMF	−3.11	1.30	−2.13	0.94	−1.76	0.79	−1.59	0.68	−1.68	0.54	−1.59	0.55	−1.76	0.55
PÉGASE, Salpeter IMF	−1.94	1.26	−1.28	0.92	−1.06	0.78	−0.85	0.62	−0.83	0.52	−0.89	0.48	−0.94	0.47
PÉGASE, $x = -1.85$ IMF	−1.52	1.16	−0.86	0.82	−0.62	0.67	−0.44	0.53	−0.41	0.42	−0.46	0.38	−0.51	0.37
PÉGASE, $x = -0.85$ IMF	−1.98	1.23	−1.44	0.94	−1.29	0.83	−0.98	0.64	−0.99	0.54	−1.04	0.49	−1.11	0.49

TABLE 4—*Continued*

Model	a_B	b_B	a_V	b_V	a_R	b_R	a_I	b_I	a_J	b_J	a_H	b_H	a_K	b_K
						$V-H$, $Z = 0.008$								
Bruzual & Charlot, Salpeter IMF	−2.39	1.17	−1.67	0.87	−1.42	0.74	−1.23	0.64	−1.10	0.51	−1.09	0.47	−1.12	0.45
Bruzual & Charlot, Scaled Salpeter IMF	−2.54	1.17	−1.83	0.87	−1.57	0.74	−1.39	0.64	−1.26	0.51	−1.25	0.47	−1.27	0.45
Bruzual & Charlot, Modified Salpeter IMF	−2.68	1.18	−1.96	0.88	−1.70	0.75	−1.53	0.65	−1.39	0.52	−1.38	0.48	−1.40	0.46
Bruzual & Charlot 96, Scalo IMF	−2.64	1.16	−1.90	0.85	−1.63	0.72	−1.46	0.63	−1.33	0.50	−1.32	0.45	−1.33	0.44
Kodama & Arimoto, Salpeter IMF	−2.38	1.14	−1.63	0.83	−1.36	0.71	−1.17	0.60	−1.02	0.48	−1.05	0.43	−1.03	0.41
Schulz et al., Salpeter IMF	−3.48	1.53	−2.48	1.13	−2.08	0.96	−1.90	0.85	−2.01	0.75	−1.90	0.73	−2.08	0.76
PÉGASE, Salpeter IMF	−2.34	1.17	−1.61	0.86	−1.36	0.74	−1.09	0.59	−1.02	0.51	−1.03	0.46	−1.08	0.46
PÉGASE, $x = -1.85$ IMF	−1.96	1.10	−1.21	0.79	−0.93	0.65	−0.70	0.52	−0.62	0.43	−0.63	0.39	−0.66	0.38
PÉGASE, $x = -0.85$ IMF	−2.23	1.08	−1.67	0.84	−1.51	0.75	−1.13	0.57	−1.09	0.49	−1.09	0.44	−1.15	0.45
						$V-H$, $Z = 0.02$								
Bruzual & Charlot, Salpeter IMF	−2.44	1.12	−1.65	0.81	−1.37	0.69	−1.19	0.59	−1.06	0.45	−1.07	0.41	−1.11	0.40
Bruzual & Charlot, Scaled Salpeter IMF	−2.59	1.12	−1.80	0.81	−1.53	0.69	−1.34	0.59	−1.21	0.45	−1.22	0.41	−1.26	0.40
Bruzual & Charlot, Modified Salpeter IMF	−2.73	1.14	−1.93	0.82	−1.66	0.69	−1.48	0.60	−1.35	0.46	−1.35	0.42	−1.39	0.41
Bruzual & Charlot 96, Scalo IMF	−2.48	1.03	−1.73	0.73	−1.47	0.62	−1.30	0.54	−1.12	0.38	−1.15	0.33	−1.15	0.32
Kodama & Arimoto, Salpeter IMF	−2.34	1.08	−1.54	0.77	−1.26	0.65	−1.07	0.54	−0.92	0.41	−0.96	0.37	−0.95	0.35
Schulz et al., Salpeter IMF	−3.22	1.31	−2.21	0.95	−1.83	0.80	−1.65	0.69	−1.73	0.55	−1.63	0.55	−1.81	0.56
PÉGASE, Salpeter IMF	−2.48	1.14	−1.67	0.83	−1.40	0.71	−1.11	0.56	−1.06	0.47	−1.09	0.43	−1.14	0.43
PÉGASE, $x = -1.85$ IMF	−2.02	1.06	−1.21	0.75	−0.91	0.61	−0.67	0.48	−0.59	0.38	−0.63	0.35	−0.67	0.34
PÉGASE, $x = -0.85$ IMF	−2.47	1.10	−1.82	0.84	−1.63	0.74	−1.24	0.57	−1.21	0.48	−1.24	0.44	−1.31	0.44
						$V-K$, $Z = 0.008$								
Bruzual & Charlot, Salpeter IMF	−2.50	1.13	−1.75	0.84	−1.48	0.71	−1.29	0.61	−1.15	0.50	−1.14	0.45	−1.16	0.44
Bruzual & Charlot, Scaled Salpeter IMF	−2.65	1.13	−1.91	0.84	−1.64	0.71	−1.45	0.61	−1.30	0.50	−1.29	0.45	−1.31	0.44
Bruzual & Charlot, Modified Salpeter IMF	−2.79	1.14	−2.04	0.85	−1.77	0.72	−1.59	0.62	−1.44	0.51	−1.42	0.46	−1.45	0.45
Bruzual & Charlot 96, Scalo IMF	−2.72	1.14	−1.95	0.83	−1.68	0.70	−1.50	0.61	−1.36	0.49	−1.35	0.44	−1.36	0.43
Kodama & Arimoto, Salpeter IMF	−2.38	1.09	−1.63	0.79	−1.36	0.67	−1.17	0.57	−1.02	0.45	−1.05	0.41	−1.03	0.39
Schulz et al., Salpeter IMF	−4.31	1.63	−3.09	1.21	−2.61	1.03	−2.36	0.91	−2.42	0.80	−2.30	0.79	−2.50	0.81
PÉGASE, Salpeter IMF	−2.51	1.16	−1.74	0.85	−1.47	0.73	−1.17	0.58	−1.10	0.50	−1.10	0.46	−1.15	0.45
PÉGASE, $x = -1.85$ IMF	−2.09	1.08	−1.30	0.77	−1.00	0.64	−0.76	0.50	−0.67	0.42	−0.68	0.38	−0.71	0.37
PÉGASE, $x = -0.85$ IMF	−2.45	1.10	−1.84	0.85	−1.66	0.76	−1.25	0.57	−1.19	0.50	−1.18	0.45	−1.25	0.45
						$V-K$, $Z = 0.02$								
Bruzual & Charlot, Salpeter IMF	−2.59	1.09	−1.76	0.79	−1.46	0.67	−1.27	0.57	−1.12	0.44	−1.12	0.40	−1.16	0.39
Bruzual & Charlot, Scaled Salpeter IMF	−2.74	1.09	−1.91	0.79	−1.62	0.67	−1.42	0.57	−1.27	0.44	−1.28	0.40	−1.32	0.39
Bruzual & Charlot, Modified Salpeter IMF	−2.88	1.10	−2.04	0.80	−1.75	0.67	−1.56	0.58	−1.41	0.45	−1.41	0.41	−1.45	0.40
Bruzual & Charlot 96, Scalo IMF	−2.53	0.98	−1.76	0.70	−1.49	0.59	−1.33	0.51	−1.14	0.36	−1.16	0.32	−1.16	0.30
Kodama & Arimoto, Salpeter IMF	−2.35	1.02	−1.55	0.73	−1.27	0.62	−1.08	0.51	−0.92	0.39	−0.97	0.35	−0.96	0.33
Schulz et al., Salpeter IMF	−3.87	1.34	−2.68	0.97	−2.23	0.81	−1.99	0.71	−2.00	0.56	−1.91	0.56	−2.09	0.57
PÉGASE, Salpeter IMF	−2.67	1.13	−1.81	0.82	−1.51	0.70	−1.21	0.56	−1.13	0.46	−1.17	0.43	−1.22	0.42
PÉGASE, $x = -1.85$ IMF	−2.17	1.04	−1.31	0.73	−0.99	0.60	−0.73	0.48	−0.64	0.38	−0.68	0.34	−0.72	0.33
PÉGASE, $x = -0.85$ IMF	−2.71	1.10	−1.99	0.84	−1.78	0.75	−1.36	0.57	−1.31	0.48	−1.33	0.44	−1.40	0.44

NOTE.—$\log_{10}(M/L) = a_\lambda + b_\lambda$ Color. Note that the stellar M/L values can be estimated for any combination of the above colors by a simple linear combination of the above fits. Table 4 is also available in machine-readable form in the electronic edition of the *Astrophysical Journal*.

(random) $\pm$ 0.2 (systematic), adopting an unweighted bisector fit. The slope will be shallower, if all disks are substantially submaximal. This is considerably shallower than the baryonic T-F relation of McGaugh et al. (2000), who advocate $L \propto V^{4\pm0.1}$. We attribute the bulk of the difference to a difference in distance scales and stellar M/L ratio normalization.

We thank Stacy McGaugh for asking us for improved stellar M/L ratio estimates for spiral galaxies, which started us off on this project. We thank all of the stellar population modelers who provided us with their models and often spent a considerable effort helping us better understand the models. We thank Roelof Bottema, Stephane Courteau, Stacy McGaugh, and the anonymous referee for helpful comments. E. F. B. was supported by NASA grant NAG5-8426 and NSF grant AST-9900789. Support for R. S. d. J. was provided by NASA through Hubble Fellowship grant HF-01106.01-A from the Space Telescope Science Institute, which is operated by the Association of Universities for Research in Astronomy, Inc., under NASA contract NAS5-26555. This research has made use of NASA's Astrophysics Data System Abstract Service and the NASA/IPAC Extragalactic Database (NED), which is operated by the Jet Propulsion Laboratory, California Institute of Technology, under contract with the National Aeronautics and Space Administration.

APPENDIX

MODEL TABLES

In this appendix we present plots of the stellar M/L ratios of the preferred model (the mass-dependent formation epoch model with bursts, with a scaled Salpeter IMF) against six colors (Fig. 9) and plots of the stellar M/L ratio against $B-R$ color for six different models (Fig. 10). We also present least-squares fits to the variation of stellar M/L ratio of a variety of different galaxy evolution and SPS models with a wide range of colors (Tables 3 and 4, respectively). Further discussion of these tables and figures are presented in the text.

REFERENCES

Bell, E. F., & Bower, R. G. 2000, MNRAS, 319, 235
Bell, E. F., & de Jong, R. S. 2000, MNRAS, 312, 497
Bessel, M. S. 1979, PASP, 91, 589
Bottema, R. 1993, A&A, 275, 16
———. 1997, A&A, 328, 517
———. 1999, A&A, 348, 77
Brinchmann, J., & Ellis, R. S. 2000, ApJ, 536, 77
Cole, S., Lacey, C. G., Baugh, C. M., & Frenk, C. S. 2000, MNRAS, 319, 168
Courteau, S., & Rix, H.-W. 1999, ApJ, 513, 561
Cox, A. N. 2000, Allen's Astrophysical Quantities (4th ed.; New York: Springer)
de Blok, W. J. G., & McGaugh, S. S. 1998, ApJ, 508, 132
de Jong, R. S. 1996, A&A, 313, 377
de Jong, R. S., & Lacey, C. 2000, ApJ, 545, 781
Disney, M. J., Davies, J. I., & Phillipps, S. 1989, MNRAS, 239, 939
Franx, M., & de Zeeuw, T. 1992, ApJ, 392, 47
Fukugita, M., Hogan, C. J., & Peebles, P. J. E. 1998, ApJ, 503, 518
Heavens, A. F., & Jimenez, R. 1999, MNRAS, 305, 770
Isobe, T., Feigelson, E. D., Akritas, M. G., & Babu, G. J. 1990, ApJ, 364, 104
Kennicutt, R. C., Jr. 1983, ApJ, 272, 54
———. 1998, ApJ, 498, 181
Kodama, T., & Arimoto, N. 1997, A&A, 320, 41
Kroupa, P. 2000, MNRAS, in press (astro-ph/0009005)
Kroupa, P., Tout, C. A., & Gilmore, G. 1993, MNRAS, 262, 545
Larson, R. B. 1999, in Star Formation 1999, ed. T. Nakamoto (Nobeyama: Nobeyama Radio Obs.), 336
Liu, M. C., Charlot, S., & Graham, J. R. 2000, ApJ, 543, 644
Matthews, L. W., van Driel, W., & Gallagher, J. S., III 1998, AJ, 116, 2196
McGaugh, S. S., Schombert, J. M., Bothun, G. D., & de Blok, W. J. G. 2000, ApJ, 533, 99
Milgrom, M., & Braun, E. 1988, ApJ, 334, 130
Moore, B., Governato, F., Quinn, T., Stadel, J., & Lake, G. 1998, ApJ, 499, L5
Navarro, J. F., & Steinmetz, M. 2000a, ApJ, 528, 607
———. 2000b, ApJ, 538, 477
Pagel, B. E. J. 1998, Nucleosynthesis and Chemical Evolution of Galaxies (Cambridge: Cambridge Univ. Press)
Parodi, B. R., Saha, A., Sandage, A., & Tammann, G. A. 2000, ApJ, 540, 634
Portinari, L., & Chiosi, C. 1999, A&A, 350, 827
Prantzos, N., & Boissier, S. 2000, MNRAS, 313, 338
Ratnam, C., & Salucci, P. 2000, NewA, 5, 427
Rocha-Pinto, H. J., Scalo, J., Maciel, W. J., & Flynn, C. 2000, A&A, 358, 869
Sakai, S., et al. 2000, ApJ, 529, 698
Salasnich, B., Girardi, L., Weiss, A., & Chiosi, C. 2000, A&A, 361, 1023
Salpeter, E. E. 1955, ApJ, 121, 61
Scalo, J. M. 1986, Fundam. Cosmic Phys., 11, 1
Schlegel, D. J., Finkbeiner, D. P., & Davis, M. 1998, ApJ, 500, 525
Schmidt, M. 1959, ApJ, 129, 243
Somerville, R. S., & Primack, J. R. 1999, MNRAS, 310, 1087
Swaters, R. A. 1999, Ph.D. thesis, Univ. Groningen
Swaters, R. A., Madore, B. F., & Trewhella, M. 2000, ApJ, 531, L107
Thuan, T. X., Izotov, Y. I., & Foltz, C. B. 1999, ApJ, 525, 105
Tinsley, B. M. 1980, Fundam. Cosmic Phys., 5, 287
Tully, R. B., & Fisher, J. R. 1977, A&A, 54, 661
Tully, R. B., & Fouqué, P. 1985, ApJS, 58, 67
Tully, R. B., & Pierce, M. J. 2000, ApJ, 533, 744
Tully, R. B., Pierce, M. J., Huang, J.-S., Saunders, W., Verheijen, M. A. W., & Witchalls, P. L. 1998, AJ, 115, 2264
van Albada, T. S., Bachall, J. N., Begeman, K., & Sancisi, R. 1985, ApJ, 295, 305
van Albada, T. S., & Sancisi, R. 1986, Philos. Trans. R. Soc. London, A, 320, 447
van den Bosch, F. C. 2000, ApJ, 530, 177
van den Bosch, F. C., Robertson, B. E., Dalcanton, J. J., & de Blok, W. J. G. 2000, AJ, 119, 1579
Verheijen, M. A. W. 1997, Ph.D. thesis, Univ. Groningen, chaps. 5 and 6
Weiner, B. J., Williams, T. B., van Gorkom, J. H., & Selwood, J. A. 2001, ApJ, 546, 916
Witt, A. N., Thronson, H. A., Jr., & Capuano, J. M., Jr. 1992, ApJ, 393, 611
Worthey, G. 1994, ApJS, 95, 107
Young, J. S., & Knezek, P. M. 1989, ApJ, 347, L55